1 **Biosynthesis and Physiological Significance of Organ-Specific Flavonol Glycosides in**

2 **Solanaceae**

3

4 **Authors**

5 Doosan Shin[1], Haohao Zhao[1], Ethan Tucker[2], Keun Ho Cho[1], Dake Liu[4], Zhixin Wang[1, 3], Scott

6 Latimer[1], Gilles Basset[1, 2], Yu Wang[1, 3], Yousong Ding[4] and Jeongim Kim[1, 2*].

7

8 **Affiliations**

9 *[1]Horticultural Sciences Department, University of Florida, 2550 Hull Rd, Gainesville, FL 32611,*

10 *USA.*

11 *[2]Plant Molecular and Cellular Biology Program, University of Florida, 2550 Hull Rd,*

12 *Gainesville, FL 32611, USA.*

13 *[3]Citrus Research & Education Center, University of Florida, 700 Experiment Station Rd, Lake*

14 *Alfred, FL 33850 USA.*

15 *[4]Department of Medicinal Chemistry, Center for Natural Products, Drug Discovery and*

16 *Development, University of Florida, 1345 Center Drive, Gainesville, FL 32610.*

17

18 **Abstract**

19 Flavonols are subclasses of flavonoids, with hundreds of structures identified in plants. This

20 chemical diversity primarily arises from glycosylation, where sugars are selectively added to the

21 flavonol backbone. While flavonol profiles vary across species and organs, the evolutionary

22 forces shaping this chemodiversity and the physiological significance of specific glycosides

23 remain a mystery. Here, we reveal that finely tuned transcriptional regulation and the sugar

24 selectivity of glycosyltransferases drive the formation of distinct organ specific flavonol profiles

25 and a specific flavonol is necessary for male fertility. In Solanaceae pollen, two flavonol

26 glycosides, K2 (kaempferol 3-*O*-glucosyl(1 → 2)galactoside) and Q2 (quercetin 3-*O*-glucosyl(1

27 → 2)galactoside), are exclusively accumulated. K2 is evolutionarily conserved, while Q2 was

28 lost over time. Consistently, K2 is essential for male fertility, whereas Q2 and aglycones fail to

29 rescue fertility defects. These findings suggest that individual flavonol glycosides have distinct

30 physiological roles, either actively maintained or discarded through evolutionary selection.

31

**Introduction**

Plants produce millions of specialized metabolites, some of which are unique to specific families or species, while others are nearly ubiquitous throughout in the plant kingdom. Flavonoids are a major class of specialized metabolites widely distributed in plants(*1*). The core structure of flavonoids, a C6-C3-C6 skeleton, consists of two aromatic rings (A and B) and a heterocyclic ring (C)(*2*). Based on the structure of the C-ring, flavonoids are classified into subclasses, including flavones, flavonols, flavanones, flavanols, anthocyanidins, and isoflavones(*2*).

Flavonols, in particular, are distinguished by their 3-hydroxyflavone backbone, which can be further modified through hydroxylation, methylation, acylation, and glycosylation resulting in various flavonol structures(*2*). For example, the flavonol aglycones kaempferol and quercetin differ by the presence or absence of a hydroxyl group at the 3′ position of the B-ring, a modification mediated by flavonoid 3′-hydroxylase (F3′H)(*3, 4*). Among these modifications, glycosylation is the most common and significantly contributes to the remarkable structural diversity of flavonols due to variations in sugar types, attachment positions, and the number of sugar units attached to aglycones(*5*). This glycosylation is primarily catalyzed by UDP-sugar dependent glycosyltransferases (UGTs), which selectively transfer sugar moieties to hydroxyl groups on flavonols(*6, 7*). These enzymes feature a conserved 44 amino acid PSPG motif in their C-terminal region that is required for glycosylation activity(*7, 8*). UGTs transfer various UDP-sugars to nucleophilic acceptor sites, typically the hydroxyl groups at positions 3, 5, 7, 3′, or 4′ on flavonol aglycones or on their glycosides, forming inter-glycosidic linkages(*9–14*). This enzymatic versatility enables plants to generate a wide range of glycosidic flavonol structures.

Although flavonols are widely present in plants, the composition and content of flavonol glycosides vary among different plant species and across various organs within a species(*15–19*). In Arabidopsis, for instance, 35 flavonol structures have been identified in various organs, which result from the glycosylation of three aglycones (kaempferol, quercetin, and isorhamnetin) decorated with various sugars such as glucose, rhamnose, and arabinose(*9*). Kaempferol glycosides carrying glucose and rhamnose accumulate ubiquitously in most organs of Arabidopsis, whereas certain flavonols such as isorhamnetin glycosides are restricted to specific organs like flowers(*9*). Quercetin 3-*O*-rhamnosyl(1→6)glucoside (rutin) is commonly found in various monocots and dicots, including buckwheat, citrus trees, apple trees, tomato, and tea

63    plants(*20–24*), but Arabidopsis does not produce rutin, although it accumulates kaempferol 3-*O*-

64    rhamnosyl(1→6)glucoside-7-*O*-rhamnoside(*9*). Despite extensive research on flavonols, it

65    remains largely unknown whether specific flavonol structures are evolutionarily conserved

66    within plant families or in specific organs and how these complex glycosylated flavonols have

67    been shaped and maintained throughout evolution.

68         Flavonols are generally recognized as antioxidants that contribute to plant stress

69    adaptation(*25*). Multiple studies have also shown that changes in flavonol content or composition

70    influence plant growth and development(*25–31*). For example, the Arabidopsis *F3'H* mutant

71    (*tt7*), which lacks quercetin and its derivatives, exhibits a slower rate of inflorescence

72    growth(*32*). Disruption of flavonol biosynthesis genes such as flavonol synthase (*FLS1*) in

73    Arabidopsis or flavonoid 3-hydroxylase (*F3H*) in tomato causes altered root architectures such as

74    lateral root and root hair development(*33, 34*). Flavonols are also known to play essential roles in

75    male fertility across various species including tomato, maize, petunia, rice, apple and tobacco(*25,*

76    *28–31, 35, 36*). In maize, *chs* mutants lacking all flavonoids showed male sterility, which was

77    rescued with flavonol aglycones, but not with anthocyanidins, flavones or flavanones(*37*).

78         Two key signaling molecules, reactive oxygen species (ROS) and auxins, are proposed to

79    be involved in flavonol-related plant growth and development phenotypes(*38, 39*). Plants with

80    reduced flavonol contents showed decreased ROS scavenging capacity, ultimately altering ROS

81    homeostasis and affecting ROS regulated plant development(*38*). Similarly, changes in flavonol

82    content or composition lead to altered auxin transport, a vital process for plant growth

83    regulation(*40*).

84         Cumulative evidence indicates the pivotal roles of flavonols in plant stress adaptation and

85    plant growth and development. However, any physiological relevance of individual flavonol

86    glycosides remains largely unexplored, although flavonols are collectively recognized as

87    antioxidants. Given the structural diversity of glycosylated flavonols, understanding any specific

88    biological significance of individual flavonol structure is crucial for unraveling their broader role

89    in plant physiology.

90         In this study, we demonstrate that two flavonols predominantly accumulate in the pollen

91    of various Solanaceae species and one of them, kaempferol 3-O-glucosyl(1 → 2)galactoside

92    (K2), is indispensable for pollen tube growth and successful seed production, while the other

93    pollen-specific flavonol, quercetin 3-O-glucosyl(1 → 2)galactoside (Q2), has been lost over time

94    without functional consequences. This pollen-specific flavonol production is driven by

95    transcriptional regulation and the constrained sugar selectivity of glycosyltransferases. This

96    study also reveals that key amino acid residues dictate the sugar specificity of a pollen-specific

97    flavonol galactosyltransferase.

98

99    **Results**

100    **Organ-specific flavonol profiles in tomato**

101         To identify flavonols accumulated in various organs of tomato, we analyzed methanol

102    soluble metabolites prepared with eleven different organs or tissues of the tomato plant (*Solanum*

103    *lycopersicum*) using High-Performance Liquid Chromatography (HPLC). The analyzed organs

104    included mature pollen grains, leaves, hypocotyls, internodes, roots, petals, sepals, as well as the

105    fruit flesh and peel of both green and red fruits. In all organs except pollen grains, two flavonol

106    rutinosides, quercetin 3-*O*-rhamnosyl(1→6)glucoside (Q-glu-rha, also known as rutin, Q4) and

107    kaempferol 3-*O*-rhamnosyl(1→6)glucoside (K-glu-rha, K4), were predominantly accumulated,

108    with Q4 (rutin) being the most abundant flavonol (Fig. 1, A and B). Among the analyzed organs,

109    red fruit peel showed the highest levels (Fig. 1B, and Fig. S2, and Table S1). However, pollen

110    showed a unique flavonol accumulation pattern. It predominantly accumulated a compound that

111    we called Peak 1, which was below the detection level in all other tested organs except petal

112    (Fig. 1, A and B). To determine the structure of this pollen specific compound, we collected the

113    HPLC eluent corresponding to the retention time of Peak 1 for MS analysis. The content of

114    eluent exhibited an *m/z* value of 611.1594 in positive mode, which corresponds to a calculated

115    exact mass of 610.1521 Da. (Fig. S1A). Further fragmentation analysis of the precursor ion

116    revealed two key fragment ions with *m/z* values of 287.0540 and 465.1009, corresponding to

117    kaempferol and kaempferol-monohexose, respectively (Fig. S1A). The *m/z* differences between

118    the parental ion and two fragments (324.1054 and 146.0512) suggest that Peak 1 represents a

119    kaempferol di-glycoside comprising two hexose units. It was previously shown that the most

120    abundant flavonol glycoside in pollen grains of petunia, a member of the Solanaceae family, is

121    kaempferol 3-*O*-glucosyl(1 → 2)galactoside (K-gal-glu), followed by quercetin 3-*O*-glucosyl(1

122    → 2)galactoside (Q-gal-glu, hereafter called Q2)(*41, 42*). We then analyzed the methanolic

123    extract of petunia pollen grains and found that the retention time and UV absorbance spectra of

124    Peak 1 exactly matched those of K-gal-glu, the most abundant peak of the petunia pollen extract

125    (Fig. S1B). Thus, we concluded that Peak 1 is kaempferol 3-*O*-glucosyl(1 → 2)galactoside (K-

126    gal-glu, hereafter called K2)(Fig. 1). This analysis also revealed that Q2 is undetectable in

127    tomato pollen, unlike in petunia pollen (Fig. S1B).

128         To detect low abundant flavonols, we reanalyzed the same methanolic soluble extracts

129    with LC-MS and detected eight flavonols that matched authentic standards: kaempferol (K),

130    quercetin (Q), K-glu (K3), Q-glu (Q3), Q-gal (Q1), K-gal (K1), K-glu-rha (K4) and Q-glu-rha

131    (Q4) (Fig. 1C). The compound having the exact mass of 610.1534 Da was again detected in

132    pollen extracts, which matches the mass of the K2 compound (Fig. S2, and Table S1). Flavonol

133    rutinosides (Q4 and K4) accumulated across various organs and their mono-glucoside precursors,

134    K-glu (K3) and Q-glu (Q3), were detected in K4 and Q4 enriched organs (Fig. 1B, and Fig. S2,

135    and Table S1). In contrast, K2 (K-gal-glu) and K1 (K-gal) accumulated predominantly in pollen

136    and two additional flavonol triglycosides (FGGG-1 and FGGG-2) were also detected in various

137    organs (Fig. S2, and Table S1).

138

139    **Identification of the enzymes responsible for the production of organ-specific flavonol**

140    **glycosides**

141         Detected flavonol glycosides contain either glucose or galactose at the 3-OH position of

142    the flavonol aglycones, kaempferol (K) or quercetin (Q) (Fig. 1, and Fig. S2), which requires

143    flavonol 3-*O*-glycosyltransferase (F3GT) activity (Fig. 1C). The production of flavonol 3-*O*-

144    diglycosides, such as K-gal-glu (K2), requires flavonol 3-*O*-glycoside: glycosyltransferase

145    (F3GGT) activity (Fig. 1C). To identify the UGTs with F3GT or F3GGT activities, we

146    conducted a phylogenetic analysis using protein sequences of 182 putative UGTs identified from

147    the tomato genome (SL4.0 build; ITAG4.0 annotation)(*43*). Our analysis also included 13

148    previously characterized F3GTs and F3GGTs from Arabidopsis, petunia, eggplant, tea, grape,

149    barley, and maize(*6, 44–53*). Two UGT homologs, Solyc10g083440 and Solyc07g006720, were

150    clustered with other characterized F3GTs in the F3GT clade (Fig. 2A). It was previously shown

151    that Solyc10g083440 (SlUGT78D-A) can convert quercetin to quercetin 3-*O*-glucoside (*24*), but

152    the function of Solyc07g006720 (hereafter called SlUGT78D-B) remains unknown. According

153    to the public database, *SlUGT78D-A* is expressed in most organs except pollen and root, whereas

154    *SlUGT78D-B* is highly expressed in pollen, which we confirmed experimentally (Fig. 2, B and

155    C).

156        Then, we conducted enzyme activity tests using recombinant SlUGT78D-A and

157        SlUGT78D-B with two sugar donors, UDP-glucose and UDP-galactose, and two sugar

158        acceptors, kaempferol and quercetin. SlUGT78D-A produced flavonol 3-*O*-glucosides (K3 and

159        Q3) or flavonol 3-*O*-galactosides (K1 and Q1) (Fig. 2D), indicating that it has both flavonol 3-*O*-

160        glucosyltransferase (F3Glu) and 3-*O*-galactosyltransferase (F3Gal) activities. In contrast,

161        SlUGT78D-B produced flavonol 3-*O*-galactosides, but not flavonol 3-*O*-glucosides, suggesting

162        that SlUGT78D-B functions as a flavonol 3-*O*-galactosyltransferase (F3Gal) but lacks 3-*O*-

163        glucosyltransferase activity (F3Glu) (Fig. 2D). It is noteworthy that flavonol 3-*O*-diglucosides,

164        K4 and Q4, were detected in pollen grains, but SlUGT78D-A having F3Glu activity is not

165        expressed in pollen grains and the pollen-specific F3GT, SlUGT78D-B, does not possess F3Glu

166        activity in vitro (Fig. 2, B and C). It appears that additional enzymes with F3Glu activity exist in

167        pollen or all 3-*O*-glucosylated flavonols such as Q4 are transported from other organs or tissues

168        like tapetum(*54*). However, our phylogenetic analysis did not identify any additional UGTs other

169        than SlUGT78D-A and SlUGT78D-B within the F3GT clade (Fig. 2A).

170        The production of K-gal-glu (K2) requires an additional UGT enzyme that can add

171        glucose to K-gal at its 2" position (2"-*O*-glucosyltransferase activity), which requires flavonol 3-

172        *O*-glycoside: glycosyltransferase (F3GGT) activity (Fig. 1C). In the F3GGT clade, five putative

173        tomato UGTs were identified (Fig. 2A). Solyc09g059170 (SlUGT79B-A) clustered closely with

174        Petunia flavonoid 3-*O*-glucoside: 6"-*O*-rhamnosyltransferase, while Solyc10g008860

175        (SlUGT79B-B) clustered with petunia flavonol 3-*O*-glycoside: 2"-*O*-glucosyltransferase. The

176        other three enzymes grouped with Arabidopsis F3GGTs (Fig. 2A). However, only *SlUGT79B-B*

177        is expressed in pollen grains, while the other four candidates show no expression in pollen grains

178        according to a public database(*55*) (Fig. 2B, and Table S2). Thus, we hypothesized that

179        SlUGT79B-B is the F3GGT responsible for K2 production in pollen grains. Indeed, recombinant

180        SlUGT79B-B showed kaempferol 3-*O*-glycoside: 2"-*O*-glucosyltransferase activity as it

181        produced K-gal-glu (K2) using K-gal and UDP-Glucose, while recombinant SlUGT79B-A did

182        not show the same activity (Fig. 2E). Our results indicate that differentially expressed flavonol

183        glycosyltransferases and their sugar specificities shape the distinctive organ-specific flavonol

184        glycoside profiles in tomato. In pollen, the repression of *SlUGT78D-A* together with the

185        activation of *SlUGT78D-B* enriches kaempferol galactosides, while the predominant activity of

186   *SlUGT78D-A* with repressed *SlUGT78D-B* results in abundant flavonol glucosides in other

187   organs (Fig. 2G).

188

**Key residues determining sugar specificity of SlUGT78D-B**

190   SlUGT78D-A and SlUGT78D-B showed not only unique organ-specific expression

191   patterns but also distinct sugar specificities, despite both enzymes having relaxed substrate

192   specificities toward flavonol aglycones (Fig. 2D). To determine the molecular basis of their

193   differing sugar preferences, we compared the amino acid sequences of SlUGT78D-A and

194   SlUGT78D-B homologs. Our analysis included the characterized CsUGT78A14 (flavonol 3-*O*-

195   glucosyltransferase, F3GluT) and CsUGT78A15 (flavonol 3-*O*-galactosyltransferase, F3GalT)

196   from *Camellia sinensis*(*51*) and five Solanaceae species (identified via an NCBI GenBank

197   BLAST search) (Fig. 3A, and Fig. S4). Phylogenetic analysis grouped the homologs into two

198   distinct clades: the F3GluT group (including SlUGT78D-A) and the F3GalT group (including

199   SlUGT78D-B) (Fig. 3A). The homologs within each group shared over 75% sequence similarity,

200   while similarity between groups was less than 50% (Fig. S4). We identified 11 amino acids

201   conserved in each group (Fig. S5), and also identified 17 residues predicted to be exposed in the

202   ligand-binding pocket based on studies of GT1 from *Vitis vinifera*(*6*, *50*) (Fig.  S5), leading us to

203   pinpoint four residues in SlUGT78D-B (14A, 19L, 138S, and 373H) which are positioned near

204   the predicted sugar binding site (Fig. 3, B and C, and Fig. S5).

205   To test the significance of the identified four residues in sugar specificity, we generated

206   various modified SlUGT78D-B proteins with substitutions at these positions using the

207   corresponding amino acids from SlUGT78D-A. SlUGT78D-B[gpaq] carrying all four amino acid

208   substitutions (A14G, L19P, S138A, H373Q) gained flavonol 3-*O*-glucosyltransferase activity

209   while retaining its galactosyltransferase activity, thereby resembling the bifunctional activity of

210   SlUGT78D-A (Fig. 3, D and E, and Fig. S6). This suggests that these residues are essential for

211   sugar specificity individually or in combination. To further narrow down key residues, we

212   generated additional modified SlUGT78D-B with single, double, and triple amino acid

213   substitutions and they all exhibited bifunctional activity, except for the single substitution at A14

214   (Fig. 3E, and Fig. S6). Given that any single amino acid substitution of L19, S138, and H373

215   enabled SlUGT78D-B to acquire glucosyltransferase activity, there is a selective pressure to

216   restrict its glucosyltransferase activity while maintaining its galactosyltransferase activity.

217 Notably, introducing the corresponding residues from SlUGT78D-B into SlUGT78D-A

218 abolished both glucosyltransferase and galactosyltransferase activities (Fig. S6), further

219 confirming their critical role for its enzymatic activities.

220

221 **Disruption of SlUGT78D-B leads to impaired pollen tube growth and reduced seed yield**

222 To determine any physiological functions of flavonol glycosides in tomato, we disrupted

223 SlUGT78D-A and SlUGT78D-B using a CRISPR/Cas9 system that simultaneously targets both

224 genes. Three independent homozygous mutant lines (named *Slugt78d-a*, *Slugt78d-b*, and

225 *Slugt78d-a/b*) were established (Fig. 4A, and Fig. S7). The *Slugt78d-a* mutant has a 4 bp deletion

226 mutation in the exon of *SlUGT78D-A*, resulting in an early stop codon, while *SlUGT78D-B*

227 remained unaltered. The *Slugt78d-b* mutant has a 2 bp deletion in the first exon of *SlUGT78D-B*

228 that causes an early stop codon. It also carries a 9 bp deletion in *SlUGT78D-A* that removes three

229 amino acids. Finally, the *Slugt78d-a/b* mutant has a 4 bp deletion in the exon of *SlUGT78D-A*

230 and a 22 bp deletion in the first exon of *SlUGT78D-B*, both resulting in early stop codons. All

231 frameshift mutations result in truncated proteins lacking the Plant Secondary Product

232 Glycosyltransferase (PSPG) motif, which is required for the glycosyltransferase reaction(*56*)

233 (Fig. S7).

234 None of the mutants exhibited any visible changes in vegetative growth or development

235 (Fig. 4B). However, both *Slugt78d-a* and *Slugt78d-a/b* mutants showed an 80% reduction in the

236 levels of flavonol glucosides, K-glu-rha (K4) and Q-glu-rha (Q4) in their leaves compared to

237 wild type and *Slugt78d-b* mutant (Fig. 4, C and D), which aligns with the flavonol 3-*O*-

238 glucosyltransferase activity of SlUGT78D-A. In contrast, the levels of K4 and Q4 in the pollen

239 of these mutants were not substantially changed compared to wild type (Fig. 4, C and D). The

240 *Slugt78d-b* mutant carries a 9 bp deletion in *SlUGT78D-A*. However, the levels of K4 and Q4

241 remained unchanged in its leaves, suggesting that the three amino acid deletion does not affect its

242 glucosyltransferase activity (Fig. 4, A, C and D). Thus, we consider *Slugt78d-b* to be a single

243 null mutant of *SlUGT78D-B*.

244 The pollen-specific flavonol, K-gal-glu (K2), was not detected in both *Slugt78d-b* and

245 *Slugt78d-a/b* pollen, whereas *Slugt78d-a* mutant accumulated wild-type levels of K2 (Fig. 4, C

246 and D) in its pollen. *SlUGT78D-A* expression was not induced in the *Slugt78d-b* pollen (Fig. S8),

247  suggesting that SlUGT78D-B is the sole enzyme responsible for the 3-*O*-galactosylation of

248  kaempferol in pollen.

249       Fruit shape and the total number of fruits per plant remained unaltered in these mutants

250  compared to wild type (Fig. 4, E and F). However, the number of seeds per plant was

251  significantly reduced in *Slugt78d-b* and *Slugt78d-a/b* compared to wild type and *Slugt78d-a* (Fig.

252  4G). As successful seed production requires effective fertilization, and flavonoid deficient

253  mutants in several species have been reported to display defective pollen(*29*, *30*, *57–59*), we

254  thought that the reduced seed yield might be related to pollen development. Interestingly, while

255  the overall shape and size of pollen grains are indistinguishable across all genotypes (Fig. S9),

256  the pollen tube lengths in *Slugt78d-b* and *Slugt78d-a/b* were significantly shorter than those in

257  wild type and *Slugt78d-a* (Fig. 4, H and I). The number of ruptured pollen tubes was also

258  increased in *Slugt78d-b* and *Slugt78d-a/b* (Fig. 4, H and J). Both *Slugt78d-b* and *Slugt78d-a/b*

259  mutants lack the pollen-specific kaempferol galactoside (K2) due to the absence of functional

260  SlUGT78D-B. It was previously shown that the tomato flavonol deficient mutant showed

261  deformed pollen grain shape and abnormal pollen tube growth, accompanied with increased

262  levels of reactive oxygen species (ROS) and the supplementation of kaempferol reduced the

263  levels of ROS and rescued defective pollen(*59*, *60*). However, we found that steady state levels

264  of free kaempferol in *Slugt78d-b* and *Slugt78d-a/b* mutants were not reduced compared to the

265  wild type (Fig. S10B). In fact, *Slugt78d-a/b* mutants accumulated a sevenfold higher level of free

266  kaempferol compared to wild type. Kaempferol aglycone is a precursor for ubiquinone, a co-

267  factor of the cellular respiration(*61–63*) (Fig. S10C). The blocked glycosylation of kaempferol in

268  the *Slugt78d-b* mutant may affect the production of ubiquinone, a lipophilic antioxidant.

269  However, the levels of ubiquinone Q10 were similar in all four genotypes (Fig. S10C).

270       Since kaempferol aglycone is not limited in *Slugt78d-b* pollen, we hypothesized that the

271  presence of kaempferol 3-*O*-galactoside or its derivatives such as K2 is associated with proper

272  pollen tube growth.

273

274  **Kaempferol galactosides, but neither aglycones nor quercetin galactosides, rescued**

275  **defective pollen tube growth**

276       Since the pollen-specific galactoside, K-gal-glu (K2), was detected in the pollen of both

277  tomato and petunia(*41*, *42*) and homologs of the K2 biosynthetic enzymes, SlUGT78D-B and

278  SlUGT79B-B, are found in other Solanaceae plants (Fig. 3A, and Fig. S4, and S11), we thought

279  that K2 might be conserved across other Solanaceae species. To test it, we analyzed methanolic

280  extracts of pollen from *Solanum tuberosum* (potato), *Capsicum annuum* (chili pepper), and two

281  tobacco species (*Nicotiana tabacum* and *Nicotiana benthamiana*) and found that K2 is the most

282  abundant flavonol in all samples (Fig. 5A, and Fig. S12). Interestingly, Q-gal-glu (Q2) was

283  detected in petunia and two tobacco species, but not in chili pepper, potato, and tomato (Fig.

284  5A). Considering that the chili pepper, potato, and tomato diverged more recently than tobacco

285  and petunia(*64*) (Fig. 5B), K2 appears to have been maintained during the evolution, whereas Q2

286  was lost over time. We showed that SlUGT78D-B can convert quercetin to quercetin 3-*O*-

287  galactoside, which can be further modified by SlUGT79B-B to produce Q2 (Fig. S1B, and S11).

288  However, tomato pollen does not accumulate Q2. One possible limiting factor is the availability

289  of quercetin in tomato pollen. F3'H activity is required for quercetin production (Fig. 1C), but

290  *SlF3'H* is not expressed in tomato pollen although it expresses in most other organs (Fig. S3).

291  Consistently, we detected *SlF3'H* expression in our leaf sample but not in pollen (Fig. 2F). This

292  suggests that distinctive pollen-specific flavonol profile is shaped through the combined

293  transcriptional regulation of key biosynthesis enzymes. Specifically, the repression of *F3'H* leads

294  to the predominance of kaempferol, while the activated *SlUGT78D-B* and the repression of

295  *SlUGT78D-A* result in enriched kaempferol galactosides in pollen (Fig. 5C and 2F).

296        To determine whether these pollen-specific flavonols play any roles in pollen tube

297  development, we conducted chemical complementation tests by supplying flavonols to

298  germinating *Slugt78d-b* pollen. When K-gal and Q-gal were supplied to the *Slugt78d-b* pollen,

299  K2 and Q2 were detected, whereas the mock control did not produce K2 and Q2 (Fig. 5d),

300  suggesting that both K-gal and Q-gal were successfully converted to K2 and Q2, respectively, in

301  pollen. Notably, K-gal supplementation increased pollen tube length and reduced the number of

302  ruptured pollen tubes in *Slugt78d-b* (Fig. 5, E and H). However, the same concentration of Q-gal

303  did not alleviate the defective pollen phenotypes (Fig. 5, E and H). We also tested various

304  concentrations of their aglycones, kaempferol and quercetin, but none of them improved the

305  defective pollen phenotypes (Fig. 5, F to H), which further confirms that kaempferol aglycone is

306  not a limiting factor for pollen tube growth, as its levels in *Slugt78d-b* pollen were seven times

307  higher than in the wild type (Fig. S10B).

308         Taken together, our findings that not all flavonols, but a specific type of flavonol

309     glycoside, effectively rescue defective pollen tube growth in tomato flavonol mutants suggest

310     physiological significance of individual flavonol structure. This may also provide a functional

311     explanation for the evolutionary loss of quercetin galactosides in certain Solanaceae species.

312

313     **Discussion**

314         Our study reveals organ-specific flavonol profiles in tomato and highlights the necessity

315     of pollen-specific kaempferol galactosides for proper pollen tube growth, which cannot be

316     compensated by other aglycones or quercetin galactosides. Multiple studies have reported

317     abnormal plant growth and development in flavonol deficient mutants in various species, often

318     attributed to impaired ROS scavenging capacity or to altered auxin transport(*33*, *38*, *60*). Our

319     data demonstrating the indispensable roles of individual flavonol structures suggests an

320     additional layer of physiological significance beyond their collective general antioxidant

321     properties. This organ-specific flavonol accumulation pattern in tomato is achieved through the

322     tight transcriptional regulation of key flavonol biosynthesis enzymes, combined with the

323     constrained sugar specificity of glycosyltransferases. Millions of specialized metabolites have

324     been identified in plants and glycosylation is a common modification across various

325     phytochemicals(*65–67*). Beyond enhancing metabolite stability or solubility, glycosylation may

326     confer specialized functions, potentially evolving to optimize plant fitness in response to

327     environmental changes.

328         In tomato, 3-*O*-glucosylated flavonols are broadly distributed across various organs and

329     tissues, but kaempferol galactosides, specifically kaempferol 3-*O*-glucosyl(1 → 2)galactoside

330     (K2), are almost exclusively enriched in pollen and not detected in most organs like leaves and

331     fruits (Fig. 1, A and B). This unique flavonol profile correlates with the distinct expression

332     patterns of flavonol 3-*O*-glycosyltransferases (UGTs) and F3'H, the flavonol 3'-hydroxylase

333     necessary for quercetin production. SlUGT78D-B having strict sugar specificity toward

334     galactose is expressed almost exclusively in pollen, whereas SlUGT78D-A having both flavonol

335     3-*O*-glucosyltransferase and galactosyltransferase activities and F3'H are ubiquitously expressed

336     across all tissues we tested except for pollen grains (Fig. 2, B and C). This differential

337     distribution of flavonol metabolites and their corresponding biosynthesis enzymes implies finely

338     tuned regulations of these metabolic pathways and possible specialized functions of each

339    individual compound in specific organs, tissues, or cells. Several transcription factors have been

340    reported to control the expression of core flavonoid biosynthetic genes, such as chalcone

341    synthase (CHS) and flavonol synthase (FLS) in Arabidopsis(*68–70*). The identity and action

342    modes of transcription regulators responsible for the organ-specific expression of flavonol

343    modification enzymes F3'H and F3GTs remain unknown. But, tight regulation of flavonol

344    modification across organs further implies significance of each flavonol structure.

345         Although our phylogenetic study did not identify any other UGTs in the F3GT clade

346    besides SlUGT78D-A and B (Fig. 2A), *Slugt78d-a* leaves still accumulated about 20% of

347    glucosylated flavonols despite the loss of functional SlUGT78D-A, indicating that other UGTs

348    may act as flavonol 3-*O*-glucosyltransferases. A previous study reported that 29 out of 91 tested

349    Arabidopsis UGTs showed quercetin glucosyltransferase activities(*48*).  Given that SlUGT78D-

350    B lacks 3-*O*-glucosyltransferase activity and SlUGT78D-A is not expressed in pollen, flavanol

351    glucosides (K4 and Q4) detected in pollen must be imported from other organs like tapetum(*71*)

352    or other UGTs having F3Glu activity must exist in pollen. Interestingly, K2 was undetectable in

353    the pollen of *Slugt78d-b* under our growth conditions. Apparently, SlUGT78D-B is the only

354    kaempferol 3-*O*-galactosyltransferase in pollen and no other promiscuous UGTs can compensate

355    for its activity in pollen.

356         Our amino acid swapping experiment identified key amino acid residues of SlUGT78D-B

357    restricting its sugar specificity. Among the four amino acids (Ala14, Leu19, Ser138, and His373)

358    predicted to face to the sugar binding pocket (Fig. 3), Leu19, Ser138, and His373 are critical to

359    restrict F3Glu activity as modifying one of them enabled SlUGT78D-B to gain F3Glu activity.

360    Despite the relaxed reversibility of sugar specificity, SlUGT78D-B remains constrained from

361    acquiring F3Glu activity while retaining its galactosyltransferase activity, reflecting an adaptive

362    advantage conferred by galactosylated kaempferol in pollen development.

363         While some Solanaceae species accumulate both K2 and quercetin 3-*O*-glucosyl(1 → 2)

364    galactoside (Q2) in their pollen, Q2 is absent in chili pepper, potato, and tomato (Fig. 5A). The

365    loss of Q2 occurred approximately 23.9 million years ago, coinciding with the separation of the

366    clade of chili pepper, potato, and tomato (Fig. 5B). Given that Q2 did not rescue the defective

367    pollen tube growth of the *Slugt78d-b* mutant (Fig. 5, E and H), Q2 may have been selectively

368    phased out.

369    K2 is conserved in Solanaceae, not all plants produce K2 in their pollen. However, each

370    species accumulates unique flavonols in their pollen. For example, Arabidopsis and Cannabis

371    accumulate kaempferol 3-*O*-glucosyl(1 → 2)glucoside (kaempferol sophoroside) or quercetin

372    sophoroside in their pollen. Similarly, flavonol sophorosides were detected in maize pollen and

373    the pollen of trees belonging to the families Juglandaceae, Betulaceae, Fagaceae, and

374    Oleaceae(*42, 72, 73*) (*10, 72–75*). Although these pollen-specific flavonol glycosides vary in

375    their decorating sugars (glucoside, galactoside) and aglycones, they have a common 1 → 2 inter-

376    glycosidic linkage (β-1→2) at the 3-OH position of aglycones. It is possible that specific

377    structure(s) of flavonols may have shared function in pollen development.

378    In general, flavonols are known as antioxidants and reactive oxygen species (ROS)

379    scavengers, critical for maintaining ROS homeostasis, which in turn affects pollen

380    development(*59, 60, 76, 77*). Consistently, tomato *f3h* mutant that is deficient in all flavonols

381    showed deformed pollen grains and defective pollen germination and tube growth accompanied

382    by increased ROS levels(*59, 60*). Supplementation with flavonol aglycones reduced ROS levels

383    and alleviate pollen defects(*59, 60*), suggesting the importance of flavonols in maintaining pollen

384    integrity. In *Slugt78d-a/b* pollen, the level of kaempferol was seven times higher than in wild

385    type (Fig. S10), yet the pollen showed defective pollen tube growth, which was not restored with

386    further supplementation of various concentration of kaempferol (Fig. 5, F to H). Instead, the

387    specific galactosylated kaempferol is critical for proper pollen tube growth in tomato (Fig. 5, F to

388    H), suggesting the physiological specificity of each flavonol structure-additional layer of

389    flavonol's function besides their general role as antioxidants. Several studies indicate that

390    flavonols may regulate auxin transport by stabilizing PIN-FORMED (PIN) protein dimers(*26,*

391    *78–81*). It is possible that specific type(s) of flavonols may affect pollen tube growth through

392    directly or indirectly interacting with molecules involving in auxin transport (*2, 35, 82*).

393    Recently, flavonol transporters were identified in rice and Arabidopsis(*54, 83*). In

394    Arabidopsis, Flavonol Sophoroside Transporter 1 (FST1) mediates localization of flavonol

395    glycosides(*54*). As it expresses in tapetum, flavonol soporosides available in tapetum can be

396    transported to pollen via FST1 and Solyc03g113440 is a putative FST1 homolog in tomato(*54*).

397    Interestingly, *Solyc03g113440* expresses exclusively in pollen grains (Fig. S13), and its role

398    remains unknown. Tomato pollen does not accumulate flavonol sophorosides, but a kaempferol

399    galactoside K2 is abundant in pollen.  K2 seems to be synthesized predominantly in pollen grains

400    rather than transported substantially from other organs or tissues, as K2 biosynthesis genes are

401    expressed in pollen grains and K2 is absent in pollen grains of *Slugt78d-b* mutants although

402    SlUGT78D-A having flavonol 3-*O*-galactosyltransferase activity functions ubiquitously in other

403    organs of *Slugt78d-b*. The tomato FST1 homolog may potentially transport flavonol glycosides

404    such as K2 or Q4 in pollen.

405         In conclusion, the exclusive accumulation of pollen-specific flavonol galactosides,

406    resulted from differentially expressed *F3'H* and *F3GTs* having distinctive sugar specificities,

407    reflects a regulatory network finely tuned to meet the developmental needs of pollen. This study

408    demonstrates that specific flavonol galactosides rather than overall abundance of total flavonols

409    matter for proper pollen tube growth and male fertility in tomato. Moreover, the loss of quercetin

410    galactosides in certain Solanaceae species suggests there are selective pressures to shape flavonol

411    composition in pollen, favoring the functional advantages conferred by kaempferol galactosides.

412    These insights advance our understanding of flavonol function in reproductive development and

413    may inform future strategies aimed at enhancing pollen viability and seed yield through targeted

414    manipulation of pollen specific flavonol glycosylation (Fig. 6).

415

**Materials and Methods**

**Plant material and growth conditions**

418    The Micro-Tom variety was used as the wild-type plant and for generating CRISPR-Cas9-

419    mediated mutant lines. All tomato plants were germinated in 3.7 x 3.7 x 5.8 cm seedling trays

420    and then transplanted into 9 x 9 x 9 cm individual pots 3 weeks after germination, where they

421    were grown until fruit and seed production. Tomato plants were grown at 22°C ± 1°C under a

422    16-hour day/8-hour night photoperiod.

423

**Generation of CRISPR-Cas9-mediated mutant lines**

425         To disrupt SlUGT78D-A and SlUGT78D-B using the CRISPR-Cas9 system, gRNAs

426    targeting both genes were designed using the CHOPCHOP software

427    (https://chopchop.cbu.uib.no/)(*84*). Specifically, two 20 bp gRNAs (5′-

428    ATTTGGGATGGCGTCAAACA-3′) and (5′-CCAAAGGGTCACGTGCTCGG-3′) were

429    selected for *SlUGT78D-A* and *SlUGT78D-B,* respectively. Then, a DNA fragment containing a

430    BsaI restriction site, the *SlUGT78D-A* gRNA, a gRNA scaffold, the U6-26t and U6-6P

431     sequences, the *SlUGT78D-B* gRNA, and another BsaI restriction site was synthesized (Twist

432     Biosciences, South San Francisco, CA, USA), which was cloned into the binary vector pHSE401

433     (Addgene, #62201) using the BsaI restriction site(*85*). The recombinant pHSE401 vector was

434     then transformed into *A. tumefaciens* strain GV3101 and inoculated into cut cotyledons

435     following a tomato transformation method[39]. The mutant lines were selected according to the

436     sequencing results of PCR products amplified with primers no. 1 and 2 for *SlUGT78D-A*, and no.

437     3 and 4 for *SlUGT78D-B* (Table S3).

438

439     **Phylogenetic analysis**

440     Putative tomato UGTs were identified by querying the UniProt database using "UDP-

441     glycosyltransferase" as the search keyword, with *Solanum lycopersicum* (taxon ID: 4081)

442     specified as the organism. Candidate sequences were further screened for the presence of the

443     PSPG (Plant Secondary Product Glycosyltransferase) domain using the NCBI Conserved

444     Domains database (https://www.ncbi.nlm.nih.gov/Structure/cdd/wrpsb.cgi). Sequences lacking

445     the PSPG domain were excluded, resulting in a final set of 182 amino acid sequences for

446     phylogenetic analysis. Previously characterized F3GTs and F3GGTs from other species (Table

447     S4) were also included in our phylogenetic analysis. All sequences were aligned using the

448     MUSCLE algorithm. Phylogenetic analysis was performed using the maximum likelihood

449     method with the Goldman +Freq. model and Gamma distribution with 5 categories in MEGA11

450     software, with 1000 bootstrap replicates. Solyc12g088170 (anthocyanin acyltransferase;

451     SlFdAT1)(*87*) was used for the outgroup in the phylogenetic analysis.

452

453     **Metabolite analysis using HPLC and LC-MS**

454     Plant samples, including pollen samples from other Solanaceae plants, were collected and

455     immediately frozen in liquid nitrogen. Soluble metabolites in the frozen samples were extracted

456     using 50% methanol at a concentration of 50 mg fresh weight/ml, except for pollen, which was

457     prepared to a concentration of 28.5 mg fresh weight/ml after 15 minutes of sonication at room

458     temperature. The extracts were centrifuged at 10,000 g for 10 minutes to remove plant tissue and

459     insoluble debris before being used for metabolite analysis. Authentic standards used for

460     metabolite identification are kaempferol, kaempferol 3-*O*-glucoside, kaempferol-3-*O*-

461     galactoside, kaempferol 3-*O*-rhamnosyl(1→6)glucoside, quercetin 3-*O*-glucoside, and quercetin

462     3-*O*-galactoside, which were obtained from Chengdu Biopurify Phytochemicals Ltd. (Chengdu,

463     China); quercetin and quercetin 3-*O*-rhamnosyl(1→6)glucoside from Sigma-Aldrich (St. Louis,

464     MO, USA); and chlorogenic acid from TCI (Portland, OR, USA).

465     For HPLC analysis, the extracts were analyzed using an UltiMate 3000 HPLC system

466     (Thermo Fisher Scientific, Waltham, MA, USA) equipped with an Acclaim™ RSLC120 C18

467     column (100 mm x 3 mm, 2.2 μm) (Thermo Fisher Scientific, Waltham, MA, USA). The mobile

468     phase consisted of solvent A (0.1% formic acid in water) and solvent B (100% acetonitrile) with

469     the following linear gradient: 5-14% B for 2.2 minutes, 14-18% B for 9 minutes, and 18-95% B

470     for 3.5 minutes, with a flow rate of 0.5 ml/min. Flavonoid contents were quantified based on

471     peak area at 345 nm using authentic standards. K-3-*O*-gal-2"-*O*-glu (K2) was quantified

472     equivalently to K-3-*O*-glu-6"-*O*-rha.

473     For Semi-targeted LC-MS analysis, an Ultimate 3000 UHPLC coupled to a TSQ

474     Quantiva triple quadrupole mass spectrometer was used (Thermo Fisher Scientific, Waltham,

475     MA, USA). 3,4,5-trihydroxycinnamic acid from Sigma-Aldrich (St. Louis, MO, USA) was used

476     as an internal standard. The injection volume for all samples was 5 μl. Analytes were eluted on

477     an Agilent InfinityLab Poroshell HPH-C18 column (2.1 × 150 mm, 1.9 μm particle size) at a

478     column temperature of 40°C using 0.1% formic acid in water (mobile phase A) and 0.1% formic

479     acid in acetonitrile (mobile phase B). A gradient elution at a flow rate of 0.4 ml/min was applied

480     as follows: 2–42% B for 28 min, 42–100% B for 2 min. The mass spectrometer operated in

481     negative ionization mode. The ESI parameters were as follows: spray voltage (positive), 3500 V;

482     spray voltage (negative), 2500 V; ion transfer tube temperature, 325°C; vaporizer temperature,

483     275°C; sheath gas, 35 Arb; aux gas, 10 Arb; and sweep gas, 0 Arb. Selective reaction monitoring

484     (SRM) was used for metabolite detection. MS/MS parameters were optimized for each

485     metabolite using flow injection analysis of individual standards. Collision-induced dissociation

486     (CID) gas pressure was set at 2 mTorr with a dwell time of 0 ms, and quadrupole resolution

487     (FWHM) was kept at 0.2. Data processing was performed using Xcalibur v4.0 (Thermo Fisher

488     Scientific, Waltham, MA, USA).

489     To identify the unknown flavonol glycoside (Peak1; K2) lacking an authentic standard

490     shown in Figure 1A, a combination of HPLC and LCMS was employed. K2 was isolated based

491     on its retention time on an HPLC system, and the isolated peak was used for further analysis.

492     Specifically, a Thermo Scientific™ Q Exactive Focus mass spectrometer coupled with a

493     Dionex™ Ultimate™ RSLC 3000 UHPLC system was used for the analysis. The system was

494     equipped with an H-ESI II probe on an Ion Max API Source. Analytes were separated on an

495     Agilent Poroshell 120 EC-C18 column (2.7 μm, 3.0 × 50 mm) using solvent A (water with 0.1%

496     formic acid) and solvent B (acetonitrile with 0.1% formic acid). The LC program with a flow

497     rate of 0.5 ml/min was as follows: 10% B for 2 min, 10-95% B over 8.5 min, 95% B for 2.5 min,

498     95% to 10% B in 0.5 min, followed by re-equilibration at 2% B for 2 min. MS signals were

499     acquired under Full MS positive ion mode, covering a mass range of m/z 150-2000, with a

500     resolution of 35,000 and an AGC target of 1E6. The precursor ion (m/z 611.1597) was selected

501     in the Orbitrap, typically with an isolation width of 3.0 m/z and fragmented in the HCD (Higher-

502     energy C-trap dissociation) cell with stepwise a collision energy (CE) of 15.

503

504     **Ubiquinone quantification**

505     Ubiquinone extraction and quantification in tomato samples were modified from

506     Ducluzeau et al(*88*). Tomato pollen samples, 0.8-1.8 mg of pollen grains, were collected and

507     spiked with 3 nmoles of ubiquinone-9. The samples were homogenized in 0.4 ml of 95% (v/v)

508     ethanol using a Pyrex tissue grinder. The grinder was rinsed twice with 0.3 ml of 95% (v/v)

509     ethanol, and washes were combined to the original extract in a 15-ml Pyrex tube containing 0.5

510     ml of water. The mixture was partitioned twice with 5 ml hexane. Hexane layers were combined,

511     evaporated to dryness with gaseous nitrogen, and resuspended in 0.2 ml of

512     ethanol:dichloromethane (10:1, v/v). Due to the pigment complexity of the pollen extracts, it was

513     not possible to fully resolve the ubiquinol-10 peak. Quinol forms were therefore converted to

514     their respective quinone counterparts by adding 1 μl of 15% $H_2O_2$. Samples were then briefly

515     centrifuged (5 min; 18,000 g) and immediately analyzed by HPLC on a 5 μm Supelco Discovery

516     C-18 column (250 × 4.6 mm, Sigma-Aldrich) thermostated at 30°C and developed in isocratic

517     mode at a flow rate of 1 ml/min with methanol:hexane (90:10, v/v). Ubiquinone forms were

518     detected spectrophotometrically at 275 nm. Retention times were 13.5 min for ubiquinone-9 and

519     18 min for ubiquinone-10 (Q10). Data were corrected for recovery of the ubiquinone-9 internal

520     standard and recovery values ranged from 79% to 95%.

521

522     **RNA extraction and expression analysis**

523       Tomato samples were collected and immediately frozen in liquid nitrogen. The samples

524    were then homogenized using a Benchmark BeadBlaster 24 homogenizer (Benchmark Scientific,

525    Edison, NJ, USA). Total RNA was extracted using TRIzol™ reagent (Life Technologies Inc.,

526    Gaithersburg, MD, USA).

527    cDNA synthesis was performed using 2 µg of total RNA and a reverse transcription kit (Thermo

528    Fisher Scientific, Waltham, MA, USA). Quantitative real-time PCR (qRT-PCR) reactions were

529    carried out using a PCR kit (Thermo Fisher Scientific, Waltham, MA, USA). Primer no. 5 and 6

530    were used for SlUGT78D-A, while primer no. 7 and 8 were used for SlUGT78D-B (Table S3).

531    The expression levels of the target genes were normalized to those of *SlACTIN2*

532    (*Solyc11g005330*) or *SlPP2Acs* (*Solyc05g006590*) as internal controls(*89*, *90*), which were

533    amplified with primer No. 9 and 10 and primer No. 11 and 12, respectively.

534

535    **Protein structure prediction**

536       To predict the protein structure of SlUGT78D-B, we employed ColabFold, a

537    computational tool that combines fast homology search with MMseqs2 and the AlphaFold2

538    algorithm(*91*). The default multiple sequence alignment (MSA) pipeline was used, which

539    included an MMseqs2 search of both the UniRef and environmental sample sequence databases.

540    The resulting predicted protein structure was saved in the Protein Data Bank (PDB) format and

541    visualized using PyMOL 2.5 (Schrödinger, LLC). To determine the ligand position, we overlaid

542    the VvGT1 structure (PDB DOI: https://doi.org/10.2210/pdb2C1Z/pdb), previously resolved via

543    crystallography (*6*), onto the predicted SlUGT78D-B enzyme structure using PyMOL 2.5.

544

545    **In vitro enzyme assay**

546       The coding sequences (CDS) of wild-type and mutant *SlUGT78D* genes were synthesized

547    by Twist Biosciences (South San Francisco, CA, USA) and introduced to the pET-28a(+) vector

548    using the NEBuilder HiFi DNA Cloning Kit (NEB, USA). The recombinants were subsequently

549    transformed into *E. coli* strain BL21 using the heat shock method. For the enzyme assay, the *E.*

550    *coli* harboring the expression vector was cultured in 50 ml of Luria broth (LB) medium at 37°C

551    with shaking at 250 rpm until the optical density at 600 nm (O.D.600) reached approximately

552    0.5. Isopropyl β-D-1-thiogalactopyranoside (IPTG) was then added to a final concentration of

553    0.1 mM to induce protein expression. After overnight incubation at 18°C, the cells were

554     harvested by centrifugation at 8000 rpm for 10 minutes at 4°C. The bacterial pellet was

555     resuspended with protein extraction buffer containing 50 mM $NaH_2PO_4 \cdot H_2O$, 300 mM NaCl,

556     10 mM imidazole, and 0.1% Triton X-100, with the pH adjusted to 8. The resuspended pellet

557     was homogenized using a Benchmark BeadBlaster 24 homogenizer (Benchmark Scientific,

558     Edison, NJ, USA) and centrifuged at 15,000 rpm for 10 minutes to obtain the supernatant. For

559     the enzyme reaction, 100 μl of the crude protein extract was mixed with 100 μl of reaction buffer

560     containing 200 mM Tris-HCl (pH 7.5), 28 mM 2-mercaptoethanol, 200 μM sugar acceptor

561     (flavonol aglycone), and 2 mM UDP-sugar. The total 200 μl reaction mixture was incubated for

562     30 minutes at 30°C, after which the reaction was stopped by adding 100% methanol. The

563     mixture was then centrifuged for 20 minutes, and 10 μl of the supernatant was injected into

564     HPLC for analysis using the same HPLC running method described in the previous section.

565

566     **Pollen tube growth assay**

567         The pollen germination and pollen tube growth assay were conducted following a

568     previously described protocol with minor modifications(*59*, *92*, *93*). Tomato pollen grains were

569     collected from newly opened flowers in the morning and immediately used the same day to

570     preserve viability. The collected pollen was incubated in Pollen Germination Medium (PGM)

571     consisting of 24% (w/v) PEG4000, 0.01% (w/v) boric acid, 2% (w/v) sucrose, 20 mM Hepes

572     buffer (pH 6.0), 30 mM $Ca(NO_3)_2$, 1.5 mM $MgSO_4$, and 1 mM $KNO_3$, on slide glasses topped

573     with cover slips.  After 4 hours of incubation at 22°C in the dark, the images of pollen tubes were

574     captured using an Olympus IX81-DSU Spinning Disk Confocal Microscope (Olympus America

575     Inc., Center Valley, PA, USA). To minimize potential discrepancies in incubation times, at least

576     three replicate slides for each condition and genotype was prepared and the order of capturing

577     confocal microscope images was rotated in each replicate and each batch. At least three

578     independent batches were examined. Pollen tube length and the number of ruptured or intact

579     pollen tubes were measured using ImageJ (ver. 1.54g for MacOS). For the flavonol feeding

580     assay, a stock solution of flavonols dissolved in DMSO was added to PGM to achieve the

581     desired final concentration, while a DMSO-only solution was used as a mock control.

582

**References**

1. K. Yonekura-Sakakibara, Y. Higashi, R. Nakabayashi, The Origin and Evolution of Plant Flavonoid Metabolism. *Frontiers in Plant Science* **10**, 943 (2019).

2. S. Alseekh, L. Perez de Souza, M. Benina, A. R. Fernie, The style and substance of plant flavonoid decoration; towards defining both structure and function. *Phytochemistry* **174**, 112347 (2020).

3. Y. Liu, J. Qian, J. Li, M. Xing, D. Grierson, C. Sun, C. Xu, X. Li, K. Chen, Hydroxylation decoration patterns of flavonoids in horticultural crops: chemistry, bioactivity, and biosynthesis. *Horticulture Research* **9**, uhab068 (2022).

4. C. Schoenbohm, S. Martens, C. Eder, G. Forkmann, B. Weisshaar, Identification of the Arabidopsis thaliana Flavonoid 3'-Hydroxylase Gene and Functional Expression of the Encoded P450 Enzyme. **381**, 749–753 (2000).

5. R. S. Khodzhaieva, E. S. Gladkov, A. Kyrychenko, A. D. Roshal, Progress and Achievements in Glycosylation of Flavonoids. *Front Chem* **9**, 637994 (2021).

6. W. Offen, C. Martinez-Fleites, M. Yang, E. Kiat-Lim, B. G. Davis, C. A. Tarling, C. M. Ford, D. J. Bowles, G. J. Davies, Structure of a flavonoid glucosyltransferase reveals the basis for plant natural product modification. *EMBO J* **25**, 1396–1405 (2006).

7. H. Gharabli, D. H. Welner, The sugar donor specificity of plant family 1 glycosyltransferases. *Front. Bioeng. Biotechnol.* **12** (2024).

8. S. A. Osmani, S. Bak, A. Imberty, C. E. Olsen, B. L. Møller, Catalytic key amino acids and UDP-sugar donor specificity of a plant glucuronosyltransferase, UGT94B1: molecular modeling substantiated by site-specific mutagenesis and biochemical analyses. *Plant Physiol* **148**, 1295–1308 (2008).

9. K. Saito, K. Yonekura-Sakakibara, R. Nakabayashi, Y. Higashi, M. Yamazaki, T. Tohge, A. R. Fernie, The flavonoid biosynthetic pathway in Arabidopsis: structural and genetic diversity. *Plant Physiol Biochem* **72**, 21–34 (2013).

10. K. Yonekura-Sakakibara, R. Nakabayashi, S. Sugawara, T. Tohge, T. Ito, M. Koyanagi, M. Kitajima, H. Takayama, K. Saito, A flavonoid 3-O-glucoside:2″-O-glucosyltransferase responsible for terminal modification of pollen-specific flavonols in Arabidopsis thaliana. *The Plant Journal* **79**, 769–782 (2014).

11. X. Dai, J. Zhuang, Y. Wu, P. Wang, G. Zhao, Y. Liu, X. Jiang, L. Gao, T. Xia, Identification of a Flavonoid Glucosyltransferase Involved in 7-OH Site Glycosylation in Tea plants (Camellia sinensis). *Sci Rep* **7**, 5926 (2017).

12. M. Peng, R. Shahzad, A. Gul, H. Subthain, S. Shen, L. Lei, Z. Zheng, J. Zhou, D. Lu, S. Wang, E. Nishawy, X. Liu, T. Tohge, A. R. Fernie, J. Luo, Differentially evolved glucosyltransferases determine natural variation of rice flavone accumulation and UV-tolerance. *Nat Commun* **8**, 1975 (2017).

13. H. Wang, C. Wang, W. Fan, J. Yang, I. Appelhagen, Y. Wu, P. Zhang, A novel glycosyltransferase catalyses the transfer of glucose to glucosylated anthocyanins in purple sweet potato. *J Exp Bot* **69**, 5444–5459 (2018).

14. Q. Yin, G. Shen, S. Di, C. Fan, Z. Chang, Y. Pang, Genome-Wide Identification and Functional Characterization of UDP-Glucosyltransferase Genes Involved in Flavonoid Biosynthesis in Glycine max. *Plant Cell Physiol* **58**, 1558–1572 (2017).

15. Y. Wang, S. K. Fong, A. P. Singh, N. Vorsa, J. Johnson-Cicalese, Variation of Anthocyanins, Proanthocyanidins, Flavonols, and Organic Acids in Cultivated and Wild Diploid Blueberry Species. *HortScience* **54**, 576–585 (2019).

16. J. C. del Valle, M. L. Buide, I. Casimiro-Soriguer, J. B. Whittall, E. Narbona, On flavonoid accumulation in different plant parts: variation patterns among individuals and populations in the shore campion (Silene littorea). *Front. Plant Sci.* **6** (2015).

17. X. Shan, Y. Li, S. Yang, Z. Yang, M. Qiu, R. Gao, T. Han, X. Meng, Z. Xu, L. Wang, X. Gao, The spatio-temporal biosynthesis of floral flavonols is controlled by differential phylogenetic MYB regulators in Freesia hybrida. *New Phytologist* **228**, 1864–1879 (2020).

18. H. Ishihara, T. Tohge, P. Viehöver, A. R. Fernie, B. Weisshaar, R. Stracke, Natural variation in flavonol accumulation in Arabidopsis is determined by the flavonol glucosyltransferase BGLU6. *Journal of Experimental Botany* **67**, 1505–1517 (2016).

19. H. Lv, S. Guo, Comparative analysis of flavonoid metabolites from different parts of Hemerocallis citrina. *BMC Plant Biology* **23**, 491 (2023).

638   20. I. Kreft, N. Fabjan, K. Yasumoto, Rutin content in buckwheat (*Fagopyrum esculentum* Moench) food
639        materials and products. *Food Chemistry* **98**, 508–512 (2006).

640   21. T. Moriguchi, M. Kita, K. Ogawa, Y. Tomono, T. Endo, M. Omura, Flavonol synthase gene
641        expression during citrus fruit development. *Physiologia Plantarum* **114**, 251–258 (2002).

642   22. J. Pandey, T. Bastola, J. Tripathi, M. Tripathi, R. K. Rokaya, B. Dhakal, R. D. C., R. Bhandari, A.
643        Poudel, Estimation of Total Quercetin and Rutin Content in Malus domestica of Nepalese Origin by
644        HPLC Method and Determination of Their Antioxidative Activity. *Journal of Food Quality* **2020**,
645        8853426 (2020).

646   23. M. Jeszka-Skowron, A. Zgoła-Grześkowiak, Analysis of Antioxidant Activity, Chlorogenic Acid,
647        and Rutin Content of Camellia sinensis Infusions Using Response Surface Methodology
648        Optimization. *Food Anal. Methods* **7**, 2033–2041 (2014).

649   24. T. Tohge, F. Scossa, R. Wendenburg, P. Frasse, I. Balbo, M. Watanabe, S. Alseekh, S. S. Jadhav, J.
650        C. Delfin, M. Lohse, P. Giavalisco, B. Usadel, Y. Zhang, J. Luo, M. Bouzayen, A. R. Fernie,
651        Exploiting Natural Variation in Tomato to Define Pathway Structure and Metabolic Regulation of
652        Fruit Polyphenolics in the Lycopersicum Complex. *Mol Plant* **13**, 1027–1046 (2020).

653   25. N. U. Kamble, Decoding the role of flavonoids in ROS management during heat stress in tomato
654        pollen. *The Plant Cell* **36**, 4285–4286 (2024).

655   26. R. Yin, K. Han, W. Heller, A. Albert, P. I. Dobrev, E. Zažímalová, A. R. Schäffner, Kaempferol 3-O-
656        rhamnoside-7-O-rhamnoside is an endogenous flavonol inhibitor of polar auxin transport in
657        Arabidopsis shoots. *New Phytol* **201**, 466–475 (2014).

658   27. P. Ramos, J. Guajardo, M. A. Moya-León, R. Herrera, A differential distribution of auxin and
659        flavonols in radiata pine stem seedlings exposed to inclination. *Tree Genetics & Genomes* **12**, 42
660        (2016).

661   28. E. H. Coe, S. M. McCormick, S. A. Modena, White pollen in maize. *Journal of Heredity* **72**, 318–320
662        (1981).

663   29. B. Ylstra, J. Busscher, J. Franken, P. C. H. Hollman, J. N. M. Mol, A. J. Van Tunen, Flavonols and
664        fertilization in Petunia hybrida: localization and mode of action during pollen tube growth. *The*
665        *Plant Journal* **6**, 201–212 (1994).

666   30.  L. Wang, L. P. Ying Lam, A. C. W. Lui, F.-Y. Zhu, M.-X. Chen, H. Liu, J. Zhang, C. Lo, Flavonoids
667        are indispensable for complete male fertility in rice. *Journal of Experimental Botany* **71**, 4715–4728
668        (2020).

669   31.  B. Ylstra, A. Touraev, R. M. B. Moreno, E. Stöger, A. J. van Tunen, O. Vicente, J. N. M. Mol, E.
670        Heberle-Bors, Flavonols Stimulate Development, Germination, and Tube Growth of Tobacco
671        Pollen. *Plant Physiology* **100**, 902–907 (1992).

672   32.  C. S. Buer, F. Kordbacheh, T. T. Truong, C. H. Hocart, M. A. Djordjevic, Alteration of flavonoid
673        accumulation patterns in transparent testa mutants disturbs auxin transport, gravity responses, and
674        imparts long-term effects on root and shoot architecture. *Planta* **238**, 171–189 (2013).

675   33.  J. M. Chapman, G. K. Muday, Flavonols modulate lateral root emergence by scavenging reactive
676        oxygen species in Arabidopsis thaliana. *Journal of Biological Chemistry* **296** (2021).

677   34.  G. S. Maloney, K. T. DiNapoli, G. K. Muday, The anthocyanin reduced Tomato Mutant
678        Demonstrates the Role of Flavonols in Tomato Lateral Root and Root Hair Development. *Plant
679        Physiology* **166**, 614–631 (2014).

680   35.  W. Chen, Z. Xiao, Y. Wang, J. Wang, R. Zhai, K. Lin-Wang, R. Espley, F. Ma, P. Li, Competition
681        between anthocyanin and kaempferol glycosides biosynthesis affects pollen tube growth and seed
682        set of Malus. *Hortic Res* **8**, 1–17 (2021).

683   36.  N. Rutley, G. Miller, F. Wang, J. F. Harper, G. Miller, M. Lieberman-Lazarovich, Enhanced
684        Reproductive Thermotolerance of the Tomato high pigment 2 Mutant Is Associated With Increased
685        Accumulation of Flavonols in Pollen. *Front. Plant Sci.* **12** (2021).

686   37.  Y. Mo, C. Nagel, L. P. Taylor, Biochemical complementation of chalcone synthase mutants defines a
687        role for flavonols in functional pollen. *Proc Natl Acad Sci U S A* **89**, 7213–7217 (1992).

688   38.  H. Daryanavard, A. E. Postiglione, J. K. Mühlemann, G. K. Muday, Flavonols modulate plant
689        development, signaling, and stress responses. *Current Opinion in Plant Biology* **72**, 102350 (2023).

690   39.  B. M. Kuhn, M. Geisler, L. Bigler, C. Ringli, Flavonols Accumulate Asymmetrically and Affect
691        Auxin Transport in Arabidopsis. *Plant Physiology* **156**, 585–595 (2011).

692  40. D. E. Brown, A. M. Rashotte, A. S. Murphy, J. Normanly, B. W. Tague, W. A. Peer, L. Taiz, G. K.
693        Muday, Flavonoids Act as Negative Regulators of Auxin Transport in Vivo in Arabidopsis. *Plant*
694        *Physiol* **126**, 524–535 (2001).

695  41. T. Vogt, L. P. Taylor, Flavonol 3-O-glycosyltransferases associated with petunia pollen produce
696        gametophyte-specific flavonol diglycosides. *Plant Physiol* **108**, 903–911 (1995).

697  42. E. Knoch, S. Sugawara, T. Mori, R. Nakabayashi, K. Saito, K. Yonekura-Sakakibara, UGT79B31 is
698        responsible for the final modification step of pollen-specific flavonoid biosynthesis in Petunia
699        hybrida. *Planta* **247**, 779–790 (2018).

700  43. Tomato Genome Consortium, The tomato genome sequence provides insights into fleshy fruit
701        evolution. *Nature* **485**, 635–641 (2012).

702  44. L. P. Taylor, W. R. Briggs, Genetic regulation and photocontrol of anthocyanin accumulation in
703        maize seedlings. *Plant Cell* **2**, 115–127 (1990).

704  45. R. P. Wise, W. Rohde, F. Salamini, Nucleotide sequence of the Bronze-1 homologous gene from
705        Hordeum vulgare. *Plant Mol Biol* **14**, 277–279 (1990).

706  46. M. Yamazaki, E. Yamagishi, Z. Gong, M. Fukuchi-Mizutani, Y. Fukui, Y. Tanaka, T. Kusumi, M.
707        Yamaguchi, K. Saito, Two flavonoid glucosyltransferases from Petunia hybrida: molecular cloning,
708        biochemical properties and developmentally regulated expression. *Plant Mol Biol* **48**, 401–411
709        (2002).

710  47. P. Jones, B. Messner, J.-I. Nakajima, A. R. Schäffner, K. Saito, UGT73C6 and UGT78D1,
711        glycosyltransferases involved in flavonol glycoside biosynthesis in Arabidopsis thaliana. *J Biol*
712        *Chem* **278**, 43910–43918 (2003).

713  48. E.-K. Lim, D. A. Ashford, B. Hou, R. G. Jackson, D. J. Bowles, Arabidopsis glycosyltransferases as
714        biocatalysts in fermentation for regioselective synthesis of diverse quercetin glucosides. *Biotechnol*
715        *Bioeng* **87**, 623–631 (2004).

716  49. S. Zhang, A. Zhang, X. Wu, Z. Zhu, Z. Yang, Y. Zhu, D. Zha, Transcriptome analysis revealed
717        expression of genes related to anthocyanin biosynthesis in eggplant (Solanum melongena L.) under
718        high-temperature stress. *BMC Plant Biol* **19**, 387 (2019).

50. E. Ono, Y. Homma, M. Horikawa, S. Kunikane-Doi, H. Imai, S. Takahashi, Y. Kawai, M. Ishiguro, Y. Fukui, T. Nakayama, Functional differentiation of the glycosyltransferases that contribute to the chemical diversity of bioactive flavonol glycosides in grapevines (Vitis vinifera). *Plant Cell* **22**, 2856–2871 (2010).

51. L. Cui, S. Yao, X. Dai, Q. Yin, Y. Liu, X. Jiang, Y. Wu, Y. Qian, Y. Pang, L. Gao, T. Xia, Identification of UDP-glycosyltransferases involved in the biosynthesis of astringent taste compounds in tea (Camellia sinensis). *Journal of Experimental Botany* **67**, 2285–2297 (2016).

52. L. M. V. Jonsson, M. E. G. Aarsman, J. Bastiaannet, W. E. Donker-Koopman, A. G. M. Geräts, A. W. Schram, Common Identity of UDP-Glucose: Anthocyanidin 3-O-Glucosyltransferase and UDP-Glucose: Flavonol 3-O-Glucosyltransferase in Flowers of Petunia hybrida. *Zeitschrift für Naturforschung C* **39**, 559–567 (1984).

53. K. D. Miller, V. Guyon, J. N. Evans, W. A. Shuttleworth, L. P. Taylor, Purification, cloning, and heterologous expression of a catalytically efficient flavonol 3-O-galactosyltransferase expressed in the male gametophyte of Petunia hybrida. *J Biol Chem* **274**, 34011–34019 (1999).

54. S. Grunewald, S. Marillonnet, G. Hause, I. Haferkamp, H. E. Neuhaus, A. Veß, T. Hollemann, T. Vogt, The Tapetal Major Facilitator NPF2.8 Is Required for Accumulation of Flavonol Glycosides on the Pollen Surface in Arabidopsis thaliana[OPEN]. *The Plant Cell* **32**, 1727–1748 (2020).

55. S. Proost, M. Mutwil, CoNekT: an open-source framework for comparative genomic and transcriptomic network analyses. *Nucleic Acids Research* **46**, W133–W140 (2018).

56. M. Wang, Q. Ji, B. Lai, Y. Liu, K. Mei, Structure-function and engineering of plant UDP-glycosyltransferase. *Comput Struct Biotechnol J* **21**, 5358–5371 (2023).

57. P. E. Pollak, K. Hansen, J. D. Astwood, L. P. Taylor, Conditional male fertility in maize. *Sexual Plant Reprod* **8**, 231–241 (1995).

58. E. G. W. M. Schijlen, C. H. R. de Vos, S. Martens, H. H. Jonker, F. M. Rosin, J. W. Molthoff, Y. M. Tikunov, G. C. Angenent, A. J. van Tunen, A. G. Bovy, RNA Interference Silencing of Chalcone Synthase, the First Step in the Flavonoid Biosynthesis Pathway, Leads to Parthenocarpic Tomato Fruits. *Plant Physiol.* **144**, 1520–1530 (2007).

746    59.  J. K. Muhlemann, T. L. B. Younts, G. K. Muday, Flavonols control pollen tube growth and integrity
747          by regulating ROS homeostasis during high-temperature stress. *PNAS* **115**, E11188–E11197 (2018).

748    60.  A. E. Postiglione, A. M. Delange, M. F. Ali, E. Y. Wang, M. Houben, S. L. Hahn, M. G. Khoury, C.
749          M. Roark, M. Davis, R. W. Reid, J. B. Pease, A. E. Loraine, G. K. Muday, Flavonols improve
750          tomato pollen thermotolerance during germination and tube elongation by maintaining ROS
751          homeostasis. *The Plant Cell*, koae222 (2024).

752    61.  E. Soubeyrand, T. S. Johnson, S. Latimer, A. Block, J. Kim, T. A. Colquhoun, E. Butelli, C. Martin,
753          M. A. Wilson, G. J. Basset, The Peroxidative Cleavage of Kaempferol Contributes to the
754          Biosynthesis of the Benzenoid Moiety of Ubiquinone in Plants. *The Plant Cell* **30**, 2910–2921
755          (2018).

756    62.  E. Soubeyrand, S. Latimer, A. C. Bernert, S. A. Keene, T. S. Johnson, D. Shin, A. K. Block, T. A.
757          Colquhoun, A. R. Schäffner, J. Kim, G. J. Basset, 3-O-glycosylation of kaempferol restricts the
758          supply of the benzenoid precursor of ubiquinone (Coenzyme Q) in Arabidopsis thaliana.
759          *Phytochemistry* **186**, 112738 (2021).

760    63.  A. Berger, S. Latimer, L. R. Stutts, E. Soubeyrand, A. K. Block, G. J. Basset, Kaempferol as a
761          precursor for ubiquinone (coenzyme Q) biosynthesis: An atypical node between specialized
762          metabolism and primary metabolism. *Current Opinion in Plant Biology* **66**, 102165 (2022).

763    64.  S. Kumar, M. Suleski, J. M. Craig, A. E. Kasprowicz, M. Sanderford, M. Li, G. Stecher, S. B.
764          Hedges, TimeTree 5: An Expanded Resource for Species Divergence Times. *Molecular Biology*
765          *and Evolution* **39**, msac174 (2022).

766    65.  J. C. D'Auria, J. Gershenzon, The secondary metabolism of Arabidopsis thaliana: growing like a
767          weed. *Curr Opin Plant Biol* **8**, 308–316 (2005).

768    66.  J. Le Roy, B. Huss, A. Creach, S. Hawkins, G. Neutelings, Glycosylation Is a Major Regulator of
769          Phenylpropanoid Availability and Biological Activity in Plants. *Front. Plant Sci.* **7** (2016).

770    67.  T. Louveau, A. Osbourn, The Sweet Side of Plant-Specialized Metabolism. *Cold Spring Harb*
771          *Perspect Biol* **11**, a034744 (2019).

772    68.  R. Stracke, O. Jahns, M. Keck, T. Tohge, K. Niehaus, A. R. Fernie, B. Weisshaar, Analysis of
773          PRODUCTION OF FLAVONOL GLYCOSIDES-dependent flavonol glycoside accumulation in

774       Arabidopsis thaliana plants reveals MYB11-, MYB12- and MYB111-independent flavonol
775       glycoside accumulation. *New Phytologist* **188**, 985–1000 (2010).

776   69. X. Zhang, Y. He, L. Li, H. Liu, G. Hong, Involvement of the R2R3-MYB transcription factor
777       MYB21 and its homologs in regulating flavonol accumulation in Arabidopsis stamen. *Journal of*
778       *Experimental Botany* **72**, 4319–4332 (2021).

779   70. T.-H. Nguyen, M. J. Kim, J. Kim, The transcription factor LBD10 sustains pollen tube growth and
780       integrity by modulating reactive oxygen species homeostasis via the regulation of flavonol
781       biosynthesis in Arabidopsis. *New Phytologist* **244**, 131–146 (2024).

782   71. E. P. Thompson, C. Wilkins, V. Demidchik, J. M. Davies, B. J. Glover, An Arabidopsis flavonoid
783       transporter is required for anther dehiscence and pollen development. *Journal of Experimental*
784       *Botany* **61**, 439–451 (2010).

785   72. S. A. Ross, M. A. ElSohly, G. N. N. Sultana, Z. Mehmedic, C. F. Hossain, S. Chandra, Flavonoid
786       glycosides and cannabinoids from the pollen of Cannabis sativa L. *Phytochemical Analysis* **16**, 45–
787       48 (2005).

788   73. F. Pratvielsosa, F. Percheron, Sophorosides of Flavonols of Some Pollens. *Phytochemistry* **11**, 1809-
789       + (1972).

790   74. E. Knoch, S. Sugawara, T. Mori, R. Nakabayashi, K. Saito, K. Yonekura-Sakakibara, UGT79B31 is
791       responsible for the final modification step of pollen-specific flavonoid biosynthesis in Petunia
792       hybrida. *Planta* **247**, 779–790 (2018).

793   75. O. Ceska, E. D. Styles, Flavonoids from Zea mays pollen. *Phytochemistry* **23**, 1822–1823 (1984).

794   76. M. Potocký, M. A. Jones, R. Bezvoda, N. Smirnoff, V. Žárský, Reactive oxygen species produced by
795       NADPH oxidase are involved in pollen tube growth. *New Phytologist* **174**, 742–751 (2007).

796   77. A. Speranza, R. Crinelli, V. Scoccianti, A. Geitmann, Reactive oxygen species are involved in pollen
797       tube initiation in kiwifruit. *Plant Biology* **14**, 64–76 (2012).

798   78. W. A. Peer, A. Bandyopadhyay, J. J. Blakeslee, S. N. Makam, R. J. Chen, P. H. Masson, A. S.
799       Murphy, Variation in Expression and Protein Localization of the PIN Family of Auxin Efflux
800       Facilitator Proteins in Flavonoid Mutants with Altered Auxin Transport in Arabidopsis thaliana.
801       *Plant Cell* **16**, 1898–1911 (2004).

79. W. A. Peer, A. S. Murphy, Flavonoids and auxin transport: modulators or regulators? *Trends in Plant Science* **12**, 556–563 (2007).

80. Z. Ding, B. Wang, I. Moreno, N. Dupláková, S. Simon, N. Carraro, J. Reemmer, A. Pěnčík, X. Chen, R. Tejos, P. Skůpa, S. Pollmann, J. Mravec, J. Petrášek, E. Zažímalová, D. Honys, J. Rolčík, A. Murphy, A. Orellana, M. Geisler, J. Friml, ER-localized auxin transporter PIN8 regulates auxin homeostasis and male gametophyte development in Arabidopsis. *Nat Commun* **3**, 941 (2012).

81. W. D. Teale, T. Pasternak, C. Dal Bosco, A. Dovzhenko, K. Kratzat, W. Bildl, M. Schwörer, T. Falk, B. Ruperti, J. V Schaefer, M. Shahriari, L. Pilgermayer, X. Li, F. Lübben, A. Plückthun, U. Schulte, K. Palme, Flavonol-mediated stabilization of PIN efflux complexes regulates polar auxin transport. *The EMBO Journal* **40**, e104416 (2021).

82. B. Pucker, D. Selmar, Biochemistry and Molecular Basis of Intracellular Flavonoid Transport in Plants. *Plants* **11**, 963 (2022).

83. Y.-C. Zhang, R.-R. He, J.-P. Lian, Y.-F. Zhou, F. Zhang, Q.-F. Li, Y. Yu, Y.-Z. Feng, Y.-W. Yang, M.-Q. Lei, H. He, Z. Zhang, Y.-Q. Chen, OsmiR528 regulates rice-pollen intine formation by targeting an uclacyanin to influence flavonoid metabolism. *Proc Natl Acad Sci U S A* **117**, 727–732 (2020).

84. K. Labun, T. G. Montague, M. Krause, Y. N. Torres Cleuren, H. Tjeldnes, E. Valen, CHOPCHOP v3: expanding the CRISPR web toolbox beyond genome editing. *Nucleic Acids Research* **47**, W171–W174 (2019).

85. H.-L. Xing, L. Dong, Z.-P. Wang, H.-Y. Zhang, C.-Y. Han, B. Liu, X.-C. Wang, Q.-J. Chen, A CRISPR/Cas9 toolkit for multiplex genome editing in plants. *BMC Plant Biology* **14**, 327 (2014).

86. J. Van Eck, P. Keen, M. Tjahjadi, "Agrobacterium tumefaciens-Mediated Transformation of Tomato" in *Transgenic Plants: Methods and Protocols*, S. Kumar, P. Barone, M. Smith, Eds. (Springer, New York, NY, 2019; https://doi.org/10.1007/978-1-4939-8778-8_16), pp. 225–234.

87. T. Tohge, Y. Zhang, S. Peterek, A. Matros, G. Rallapalli, Y. A. Tandrón, E. Butelli, K. Kallam, N. Hertkorn, H.-P. Mock, C. Martin, A. R. Fernie, Ectopic expression of snapdragon transcription factors facilitates the identification of genes encoding enzymes of anthocyanin decoration in tomato. *The Plant Journal* **83**, 686–704 (2015).

88. A.-L. Ducluzeau, Y. Wamboldt, C. G. Elowsky, S. A. Mackenzie, R. C. Schuurink, G. J. C. Basset, Gene network reconstruction identifies the authentic trans-prenyl diphosphate synthase that makes the solanesyl moiety of ubiquinone-9 in Arabidopsis. *The Plant Journal* **69**, 366–375 (2012).

89. B. J. W. Dekkers, L. Willems, G. W. Bassel, R. P. (Marieke) van Bolderen-Veldkamp, W. Ligterink, H. W. M. Hilhorst, L. Bentsink, Identification of Reference Genes for RT–qPCR Expression Analysis in Arabidopsis and Tomato Seeds. *Plant and Cell Physiology* **53**, 28–37 (2012).

90. C. Sun, L. Deng, M. Du, J. Zhao, Q. Chen, T. Huang, H. Jiang, C.-B. Li, C. Li, A Transcriptional Network Promotes Anthocyanin Biosynthesis in Tomato Flesh. *Molecular Plant* **13**, 42–58 (2020).

91. M. Mirdita, K. Schütze, Y. Moriwaki, L. Heo, S. Ovchinnikov, M. Steinegger, ColabFold: making protein folding accessible to all. *Nat Methods* **19**, 679–682 (2022).

92. Z. Weng, Y. Deng, F. Tang, L. Zhao, L. Zhao, Y. Wang, X. Dai, Z. Zhou, Q. Cao, Screening and optimisation of in vitro pollen germination medium for sweetpotato (Ipomoea batatas). *Plant Methods* **19**, 93 (2023).

93. D. Tushabe, S. Rosbakh, A Compendium of in vitro Germination Media for Pollen Research. *Front. Plant Sci.* **12** (2021).

## Acknowledgments

863    **Competing interests**

864    The authors declare a potential conflict of interest as this research covers aspects of a provisional

865    patent application (U.S. Provisional Application No. 63/776,657, filed on March 24, 2025).

866

867    **Figures and Tables**

868    **Fig. 1. Flavonol profiling with eleven tomato organs and tissues reveals pollen-specific**

869    **compounds.**

870    **(A)** Representative HPLC chromatograms of methanolic extracts from eleven tomato organs and

871    tissues, together with authentic standards of four 3-*O*-glucosylated flavonols (K3, K4, Q3, and

872    Q4) and two flavonol 3-*O*-galactosides (K1 and Q1). The pollen extract shown in the

873    chromatogram was extracted in 50% methanol at a concentration approximately 6.2 times more

874    diluted compared to other organs. Peak 1 indicated with a blue dot is highly accumulated in

875    pollen grains, while no peak 1 was detected in the rest of samples. Peak 1 characterized as K2

876    (kaempferol 3-*O*-glucosyl(1→2)galactoside) in Figure S1. Chlorogenic acid, a caffoylquinate,

877    are marked in the chromatograms. **(B)** Quantification of three major flavonol glycosides (K2, K4

878    and Q4) across different tomato organs detected with HPLC. The data presented are the mean

879    concentrations (pmol mg$^{-1}$ fresh weight) of flavonol glycosides and their standard deviations (n =

880    4). Compounds that were below the detection limit in certain organs are marked as not detected

881    (n.d.). **(C)** Simplified biosynthetic pathway of flavonol glycosides in tomato. Flavonol

882    biosynthesis begins with the conversion of phenylalanine into dihydroflavonols, mediated by

883    several enzymatic steps. Dihydroflavonols are then converted to flavonols (kaempferol and

884    quercetin) by flavonol synthase (FLS). Kaempferol (K) and quercetin (Q) undergo glycosylation

885    by flavonol 3-*O*-glycosyltransferases (F3GT), leading to the production of initial glycosylated

886    intermediates, such as kaempferol 3-*O*-galactoside (K-gal; K1), kaempferol 3-*O*-glucoside (K-

887    glu; K3), quercetin 3-*O*-galactoside (Q-gal; Q1), and quercetin 3-*O*-glucoside (Q-glu; Q3). These

888    intermediates are further modified by flavonol 3-*O*-glycoside: glycosyltransferases (F3GGT),

889    generating secondary glycosides, including kaempferol 3-*O*-glucosyl(1→2)galactoside (K-gal-

890    glu; K2), kaempferol 3-*O*-glucosyl(1→6)rhamnoside (K-glu-rha; K4), quercetin 3-*O*-

891    glucosyl(1→2)galactoside (Q-gal-glu; Q2), and quercetin 3-*O*-glucosyl(1→6)rhamnoside (Q-

892    glu-rha; Q4). Abbreviations used in chemical structures are K, kaempferol; Q, quercetin; gal,

893    galactose; glu, glucose; rha, rhamnose.

894

895    **Fig. 2. Identification of two UGT enzymes responsible for a pollen-specific flavonol**

896    **glycosides.**

897    **(A)** A phylogenetic tree of UDP-Glycosyltransferases (UGTs). A phylogenetic tree constructed

898    using 182 UGT protein sequences retrieved from the tomato genome and previously

899    characterized F3GTs and F3GGTs from other species (Table S4). The tree was generated using

900    the maximum likelihood method with 1000 bootstrap replicates and WAG with Freqs. (+F)

901    model. Solyc12g088170 (anthocyanin acyltransferase; SlFdAT1) was used as an outgroup. Two

902    zoom-in clades representing the F3GT and the F3GGT clades are shown in purple and green,

903    respectively. **(B)** Heatmap showing the normalized expression (TPM) of *UGT* genes in different

904    tomato organs, including roots, stems, leaves, flowers, and fruits. Particularly, *SlUGT78D-B* and

905    *SlUGT79B-B* show expression in pollen while other flavonol UGT homologs do not. The

906    expression data were sourced from a public database (https://conekt.sbs.ntu.edu.sg)(*91*) and raw

907    expression data are available in Table S2. **(C)** The relative gene expression levels of *SlUGT78D-*

908    *A* and *SlUGT78D-B* in different tomato organs, measured by qRT-PCR. Expression was

909    normalized to *SlPP2Acs* (*Solyc05g006590*) an internal control. The data are presented as mean ±

910    SD (n = 3). n.d. indicates not detected **(D)** In vitro enzymatic assays of SlUGT78D-A and

911    SlUGT78D-B. HPLC chromatograms of enzyme reaction mixtures demonstrate the production

912    of K-glu (K3), Q-glu (Q3), K-gal (K1), and Q-gal (Q1) when SlUGT78D-A and SlUGT78D-B

913    were incubated with two flavonol aglycones, kaempferol (K) and quercetin (Q), and two sugar

914    donors, UDP-glucose and UDP-galactose. SlUGT78D-A shows both glucosyltransferase and

915    galactosyltransferase activities at the 3-OH position on kaempferol and quercetin, while

916    SlUGT78D-B exhibits galactosyltransferase activity, but no glucosyltransferase activity.

917    Chromatograms were obtained at a wavelength of 345 nm. **(E)** HPLC chromatograms showing

918    the enzymatic activity of SlUGT79B-B, which produces K-gal-glu (K2) from K-gal using UDP-

919    glucose as sugar donor. SlUGT79B-A does not show this activity. The chromatograms were

920    obtained at a wavelength of 345 nm. **(F)** Working model of transcriptional regulation of key

921   enzymes determining the distinct flavonol glycoside profiles between pollen and other organs. In

922   organs outside of pollen, flavonoid 3'-hydroxylase (F3'H) is active, producing both kaempferol

923   and quercetin, which are glucosylated by SlUGT78D-A to form flavonol 3-*O*-glucosides (F-glu).

924   Further glycosylation by SlUGT79B-A results in the formation of flavonol 3-*O*-

925   glucosyl(1→6)rhamnoside (F-glu-rha; Q4, K4). In pollen, however, F3'H expression is

926   repressed, and galactosylation becomes predominant due to the activation of SlUGT78D-B and

927   repression of SlUGT78D-A. This switch leads to the production of kaempferol 3-*O*-galactoside

928   (K-gal). Further modification by SlUGT79B-B results in kaempferol 3-*O*-

929   glucosyl(1→2)glucoside (K2), which is uniquely abundant in pollen. Abbreviations are K,

930   kaempferol; Q, quercetin; UDP-Glu, UDP-glucose; UDP-Gal, UDP-galactose; glu, glucose; gal,

931   galactose; rha, rhamnose.

932

933   **Fig. 3. Identification of key amino acids for sugar specificity in SlUGT78D-B.**

934   **(A)** Phylogenetic analysis with SlUGT78D-A and SlUGT78D-B homologs from Solanaceae

935   species shows two distinct groups, the SlUGT78D-A group and the SlUGT78D-B group, which

936   are highlighted in red and blue, respectively. The tree was constructed using the maximum

937   likelihood method with a bootstrap analysis of 1000 replicates, using the WAG with Freqs. (+F)

938   model. Tomato F3GGT enzymes, SlUGT79B-B and SlUGT79B-A, are used as the outgroup.

939   **(B)** Sequence alignment of F3GTs showing four amino acid residues conserved in each group,

940   which are highlighted in red and blue for the SlUGT78D-A group and the SlUGT78D-B group,

941   respectively. Amino acids positions 14, 19, 138, and 373 are indicated based on the SlUGT78D-

942   B sequences. **(C)** A structural model of SlUGT78D-B was generated with ColabFold(*91*) and

943   visualized with PyMOL2.5. The ligand position was determined according to the VvGT1

944   structure (PDB DOI: https://doi.org/10.2210/pdb2C1Z/pdb). Amino acids targeted for point

945   mutations are highlighted in green. **(D)** HPLC chromatograms showing the activity of wild-type

946   SlUGT78D-B (B[ALSH]) and mutated SlUGT78D-B (B[gpaq]) with kaempferol and quercetin

947   substrates, using UDP-galactose and UDP-glucose as sugar donors. The wild-type enzyme

948   (B[ALSH]) shows galactosyltransferase activity, but no glucosyltransferase activity, while the

949   quadruple mutant (B[gpaq]) acquires glucosyltransferase activity, producing K-3-*O*-glu and Q-3-*O*-

950   glu. The HPLC chromatograms were obtained at a wavelength of 345 nm. **(E)** The

951   glucosyltransferase and galactosyltransferase activities of SlUGT78D-B mutant variants.

952    Activities are shown for quadruple, triple, double, and single mutants at positions 14, 19, 138,

953    and 373. The presence of activity is indicated with multiple (+) marks based on product peak

954    area in HPLC analysis (a higher number of '+' marks indicate a greater level of the detected

955    product compound), and the absence of activity is indicated with "n.d." (not detected).

956

957    **Fig. 4. Disruption of SlUGT78D-B abolishes pollen kaempferol galactosylation, leading to**

958    **defective pollen tube development and lower seed yield**

959    **(A)** Schematic gene structures of *SlUGT78D-A* and *SlUGT78D-B* with the CRISPR-Cas9

960    targeting sites and mutations in *Slugt78* mutants. PSPG motif is marked on gene structures with a

961    blue box. The guide RNA (gRNA) binding sites and the protospacer adjacent motif (PAM) are

962    highlighted in yellow and green, respectively. The resulting deletion mutations in the mutant

963    lines (*Slugt78d-a*, *Slugt78d-b*, and *Slugt78d-a/b*) are indicated. **(B)** Representative images of 3-

964    week-old wild type (WT), *Slugt78d-a*, *Slugt78d-b*, and *Slugt78d-a/b*. Scale bar = 3 cm.

965    **(C)** Representative HPLC chromatogram of methanolic extracts from leaves (green traces) and

966    pollen (brown traces) of 4-week-old wild type (WT), *Slugt78d-a*, *Slugt78d-b*, and *Slugt78d-*

967    *a/b* mutants. The retention times for kaempferol 3-O-glucosyl(1→2)galactoside (K2), quercetin

968    3-O-glucosyl(1→6)rhamnoside (Q4), and kaempferol 3-O-glucosyl(1→6)rhamnoside (K4) are

969    indicated on the chromatogram. The compound structure at the top of the graph are identified by

970    their abbreviations: K for kaempferol, Q for quercetin, glu for glucose, gal for galactose, and rha

971    for rhamnose. **(D)** The levels of K2, Q4 and K4 in leaves and pollen from wild type (WT) and

972    three mutant lines. Methanolic extracts were analyzed with HPLC, and the concentration is

973    shown in peak area per fresh weight (mAU*min FW$^{-1}$). Data represent mean ± SD (n=3).

974    Statistical significance was determined using one-way ANOVA, followed by Tukey's post-hoc

975    test, with different letters indicating significant differences among groups (P-value < 0.05). Each

976    data point is shown as an open circle on the bar graph. n.d. indicates not detected. **(E)** Cross-

977    sectioned fruits of WT, *Slugt78d-a*, *Slugt78d-b*, and *Slugt78d-a/b*. **(F,G)** Bar graph showing the

978    average number of fruits per plant (f), and the number of seeds per plant (g) Data represent mean

979    ± SD (n=12 for all groups except *Slugt78d-a/b*, where n=3). **(H)** Microscopic images of growing

980    pollen tubes in WT, *Slugt78d-a*, *Slugt78d-b*, and *Slugt78d-a/b*. Red arrows indicate ruptured

981    pollen tubes. Scale bar = 200 μm. **(I)** Violin plot showing pollen tube length for WT, *Slugt78d-a*,

982    *Slugt78d-b*, and *Slugt78d-a/b* (n = 200). **(J)** Bar graph showing the percentage of ruptured

983     pollens. Data represent mean ± SD (n=5 with each replicate containing approximately 100 pollen

984     grains**). (F-G, I-J)** Each data point is shown as a circle. Statistical significance was determined

985     using one-way ANOVA, followed by Dunnett's multiple comparisons test, with adjusted P-

986     values marked at the top.

987

988     **Fig. 5. Selective rescue of pollen tube defects by galactosylated kaempferol and its**

989     **evolutionary implications for galactosylated quercetin loss in late-diverged Solanaceae**

990     **(A)** HPLC chromatograms showing the presence of quercetin 3-*O*-glucosyl(1→2)galactoside

991     (Q2) and kaempferol 3-*O*-glucosyl(1→2)galactoside (K2) in pollen extracts from six Solanaceae

992     plants including *Petunia hybrida* (*P. hybrida*), *Nicotiana benthamiana* (*N. benthamiana*),

993     *Nicotiana tabacum* (*N. tabacum*), *Capsicum annuum* (*C. annuum*), *Solanum tuberosum* (*S.*

994     *tuberosum*), and *Solanum lycopersicum* (*S. lycopersicum*). The K2 peak was detected in

995     methanolic extracts of all six Solanaceae pollens, while Q2 was detected only in petunia and two

996     tobacco species. The HPLC chromatograms were obtained at a wavelength of 345 nm.

997     **(B)** Phylogenetic tree depicting speciation within the Solanaceae family. The tree illustrates the

998     divergence times (in millions of years ago, MYA) among Solanaceae species shown in (a).

999     Divergence times are labeled at each node. The phylogenetic tree was retrieved from TimeTree,

1000     a web-based database (https://timetree.org). The scale bar represents 5 million years (MYA).

1001     **(C)** The relative gene expression levels of *SlF3'H* in pollen and leaf, measured by qRT-PCR.

1002     Expression was normalized to *SlPP2Acs* (*Solyc05g006590*) an internal control. The data are

1003     presented as mean ± SD (n = 3). n.d. indicates not detected**. (D)** Conversion of flavonol

1004     monoglycosides to flavonol diglycosides in *Slugt78d-b* mutant pollen in chemical

1005     complementation. HPLC chromatograms show the conversion of kaempferol 3-*O*-galactoside

1006     (K-gal) to kaempferol 3-*O*-glucosyl(1→2)galactoside (K2) in the left panel, and quercetin 3-*O*-

1007     galactoside (Q-gal) to quercetin 3-*O*-glucosyl(1→2)galactoside (Q2) in the right panel,

1008     in *Slugt78d-b* pollen treated with 200 μM flavonol monoglycosides. Pollen treated with the same

1009     volume of DMSO (mock control) did not produce detectable levels of Q2 or K2. After flavonol

1010     monoglycoside treatment in PGM media, metabolites were extracted using a methanolic solution

1011     following 4 hours of incubation. Chromatograms were extracted at a wavelength of 345 nm,

1012     confirming the formation of flavonol diglycosides. **(E)** Violin plot showing the pollen tube

1013     length (n = 200) of *Slugt78d-b* pollen treated with 200 μM flavonol monoglycosides (kaempferol

1014    3-*O*-galactoside, K-gal; and quercetin 3-*O*-galactoside, Q-gal) or an equivalent volume of

1015    DMSO (mock). **(F, G)** Violin plots showing the pollen tube length of *Slugt78d-b* pollen treated

1016    with varying concentrations (1 μM, 50 μM, and 200 μM) of kaempferol (K) and quercetin (Q)

1017    aglycones (n = 200). **(H)** Bar graph illustrating the percentage of ruptured pollen tubes (n = 5,

1018    with each replicate containing approximately 100 pollen grains) in *Slugt78d-b* pollen

1019    supplemented with 200 μM flavonols or an equivalent amount of DMSO (mock). **(E-H)** Each

1020    data point is represented by a circle on the violin or bar graphs. Statistical significance was

1021    determined using one-way ANOVA followed by Dunnett's multiple comparisons test, with

1022    adjusted P-values displayed above the comparisons.

1023

1024    **Fig. 6. Working model depicting the role of flavonol glycosylation in successful fertilization.**

1025    **(A)** Organ-specific flavonol glycoside biosynthesis pathways in tomato pollen and other organs.

1026    In pollen, kaempferol (K) is synthesized from dihydrokaempferol via flavonol synthase (FLS).

1027    The glycosyltransferase SlUGT78D-B catalyzes the formation of kaempferol 3-*O*-galactoside

1028    (K-gal, K1), which is further modified by SlUGT79B-B to produce kaempferol 3-*O*-galactoside-

1029    2"-*O*-glucoside (K-gal-glu, K2), a pollen-specific flavonol glycoside. In other organs,

1030    kaempferol (K) and quercetin (Q) are produced via FLS, with F3'H catalyzing the conversion of

1031    dihydrokaempferol to dihydroquercetin, a precursor of quercetin. These flavonols are

1032    glycosylated by SlUGT78D-A to form kaempferol 3-*O*-glucoside (K-glu, K3) and quercetin 3-*O*-

1033    glucoside (Q-glu, Q3). Further modification by SlUGT79B-A produce kaempferol 3-*O*-

1034    glucosyl(1→6)rhamnoside (K-glu-rha, K4) and quercetin 3-*O*-glucosyl(1→6)rhamnoside (Q-

1035    glu-rha, Q4), which are abundant in vegetative tissues. **(B)** Schematic illustration of pollen tube

1036    growth defects in *Slugt78d-b* mutants and chemical complementation analysis. Wild-type (WT)

1037    pollen accumulates kaempferol (K) and its glycosylated derivatives, including K1 (kaempferol 3-

1038    *O*-galactoside) and K2 (kaempferol 3-*O*-galactoside-2"-*O*-glucoside), which are essential for

1039    normal pollen tube growth. In *Slugt78d-b* mutant pollen, the absence of K1 and K2 results in

1040    defective pollen tube growth, as observed in the mock treatment. Chemical complementation was

1041    conducted by supplementing *Slugt78d-b* mutant pollen with various flavonol derivatives. Among

1042    the tested compounds, only the addition of K1 successfully rescued the pollen tube growth defect

1043    by restoring K2 biosynthesis. In contrast, complementation with Q1 (quercetin 3-*O*-galactoside),

1044    K, or Q failed to restore normal pollen tube growth. **(C)** Schematic illustration of reduced seed

1045     production caused by defective pollen tube growth in *Slugt78d-b* mutants. In WT plants, pollen

1046     tubes successfully germinate and grow through the style, delivering male genetic material to the

1047     ovules in the ovary, resulting in normal seed production. In contrast, *Slugt78d-b* mutant pollen

1048     exhibits defective pollen tube growth, impairing fertilization and significantly reducing seed

1049     production. This schematic highlights the critical role of *SlUGT78D-B* in regulating pollen tube

1050     development and ensuring efficient seed production in tomato.

1051

1052     **Supplementary Materials**

1053     Supplementary Figure S1: Identification of a pollen specific kaempferol 3-*O*-glucosyl(1 →

1054     2)galacoside in tomato pollen grains.

1055     Supplementary Figure S2: Heatmap of flavonol glycosides across tomato organs detected with

1056     LC-MS.

1057     Supplementary Figure S3: Gene expression profile of *SlF3'H* (*Solyc03g115220*).

1058     Supplementary Figure S4: Homologs of flavonol 3-*O*-glycosyltransferase enzymes (SlUGT78D-

1059     A and SlUGT78D-B) in other Solanaceae species.

1060     Supplementary Figure S5: Protein sequence alignment of F3GTs.

1061     Supplementary Figure S6: Enzyme activities of modified F3GT enzymes.

1062     Supplementary Figure S7: Generation of *Slugt78d-a*, *Slugt78d-b*, and *Slugt78d-a/b* mutants using

1063     the CRISPR-Cas9 system.

1064     Supplementary Figure S8: *SlUGT78D-A* is not transcriptionally induced in *Slugt78d-b* pollen.

1065     Supplementary Figure S9: Pollen grain morphology in wild type and three *Slugt78d* mutants.

1066     Supplementary Figure S10: Ubiquinone Q10 content in pollen grains.

1067     Supplementary Figure S11. Homologs of flavonol 3-*O*-glycoside: glycosyltransferase (F3GGT)

1068     enzymes (SlUGT79B-A and SlUGT79B-B) in other Solanaceae species.

1069     Supplementary Figure S12: Conservation of pollen-specific kaempferol 3-*O*-glucosyl(1 →

1070     2)galactoside (K2).

1071     Supplementary Figure S13: Gene expression profile of *SlFST1* (*Solyc03g113440*) a homolog of

1072     Arabidopsis *FST1*.

1073     Supplementary Table S1. LC-MS organ metabolite profile.

1074     Supplementary Table S2. Gene expression profile depending on organs

1075     Supplementary Table S3. Primer list used in this study.

1076      Supplementary Table S4. Protein accession number for phylogenetic tree.

1077
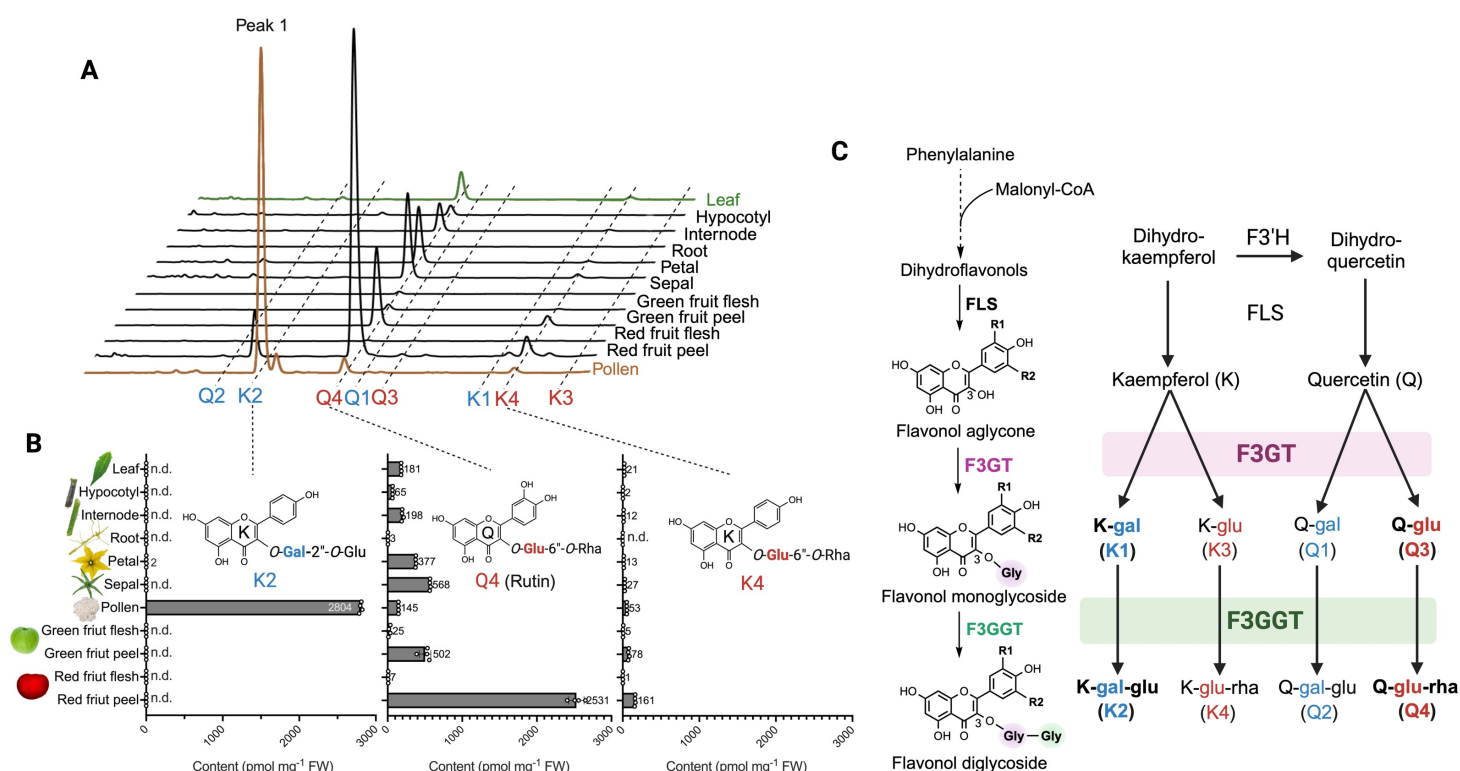
1078

**Fig. 1. Flavonol profiling with eleven tomato organs and tissues reveals distinct organ-specific flavonol accumulation patterns.**

**(A)** Representative HPLC chromatograms of methanolic extracts from eleven tomato organs and tissues, together with authentic standards of four 3-*O*-glucosylated flavonols (K3, K4, Q3, and Q4) and two 3-*O*-galactosylated flavonols (K1 and Q1). Peak 1 indicated a compound that accumulates highly in pollen grains, which was identified as K2 (kaempferol 3-*O*-glucosyl(1→2)galactoside), as shown in Supplementary Figure S1. Retention time of Q2 was determined based on that of Q2 in the Petunia pollen extract shown in Supplementary Figure S1b. **(B)** Quantification of three major flavonol glycosides (K2, K4 and Q4) across different tomato organs detected with HPLC. The data are presented as the mean concentrations (pmol mg⁻¹ fresh weight) of flavonol glycosides, with standard deviations (n = 4) shown as error bars. Each data point is marked with an open circle. 'n.d.' means not detected. **(C)** Simplified biosynthetic pathway of flavonol glycosides in tomato. Flavonol biosynthesis begins with the production of dihydrokaempferol, which can be hydroxylated to make dihyroquercetin. Both dihydrokaempferol and dihydroquercetin are then converted to flavonol aglycones kaempferol and quercetin by flavonol synthase (FLS). Kaempferol (K) and quercetin (Q) undergo glycosylation by flavonol 3-*O*-glycosyltransferases (F3GT) leading to the production of flavonol monoglycosides, such as kaempferol 3-*O*-galactoside (K-gal; K1), kaempferol 3-*O*-glucoside (K-glu; K3), quercetin 3-*O*-galactoside (Q-gal; Q1), and quercetin 3-*O*-glucoside (Q-glu; Q3). They are further modified by flavonol 3-*O*-glycoside: glycosyltransferases (F3GGT) to produce flavonol diglycosides, including kaempferol 3-*O*-glucosyl(1→2)galactoside (K-gal-glu; K2), kaempferol 3-*O*-rhamnosyl(1→6)glucoside (K-glu-rha; K4), quercetin 3-*O*-glucosyl(1→2)galactoside (Q-gal-glu; Q2), and quercetin 3-*O*-rhamnosyl(1→6)glucoside (Q-glu-rha; Q4). Abbreviations used in chemical structures are K, kaempferol; Q, quercetin; gal, galactose; glu, glucose; rha, rhamnose. Kaempferol has hydrogen (H) at both R1 and R2, whereas quercetin has H at R1 and a hydroxyl group (OH) at R2.
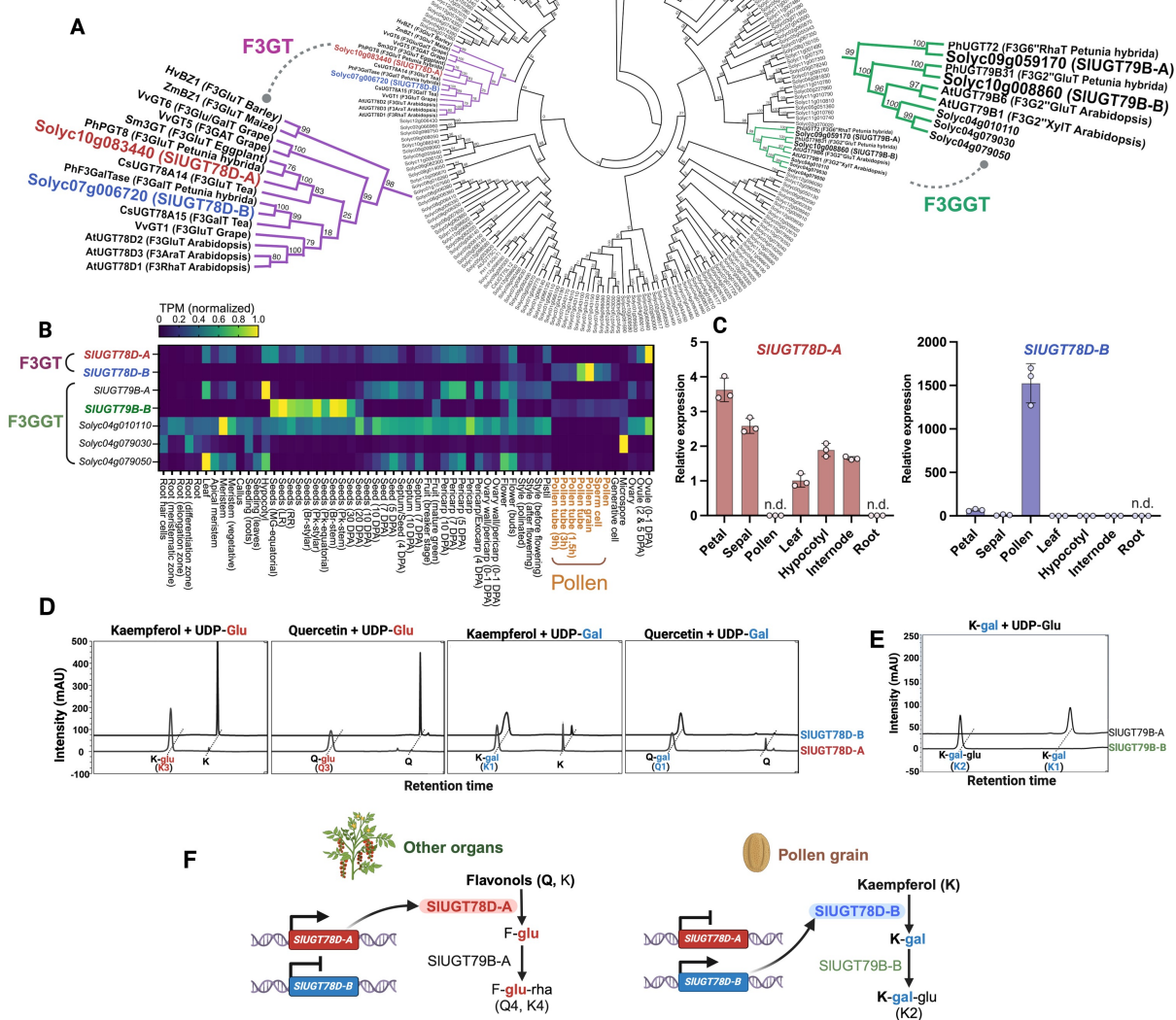
**Fig. 2. Identification of UGT enzymes responsible for the production of organ-specific flavonol glycosides.**
**(A)** A phylogenetic tree of UDP-Glycosyltransferases (UGTs). A phylogenetic tree constructed using 182 putative UGT protein sequences retrieved from the tomato genome and previously characterized F3GTs and F3GGTs from other species (Supplemental Table S4). The tree was generated using the maximum likelihood method with 1000 bootstrap replicates and WAG with Freqs. (+F) model. Solyc12g088170 (anthocyanin acyltransferase; SlFdAT1) was used as an outgroup. Two zoom-in clades representing the F3GT and the F3GGT clades are shown in purple and green, respectively. **(B)** Heatmap showing the normalized expression (TPM) of two F3GT and five F3GGT candidate genes in different tomato organs, including roots, stems, leaves, flowers, and fruits. Particularly, *SlUGT78D-B* and *SlUGT79B-B* show expression in pollen while the rest of identified flavonol UGT homologs do not. The expression data were sourced from a public database (https://conekt.sbs.ntu.edu.sg)[55] and raw expression data are available in Supplemental Table S2. **(C)** The relative expression of *SlUGT78D-A* and *SlUGT78D-B* in different tomato organs was measured by qRT-PCR. Expression was normalized to *SlPP2Acs* (*Solyc05g006590*), an internal control. The data are presented as mean ± SD (n = 3). n.d. indicates not detected. Each data point is marked on the bar as an open circle. **(D)** In vitro enzymatic assays of SlUGT78D-A and SlUGT78D-B. HPLC chromatograms of enzyme reaction mixtures demonstrate the production of K-glu (K3), Q-glu (Q3), K-gal (K1), and Q-gal (Q1) when SlUGT78D-A and SlUGT78D-B were incubated with two flavonol aglycones, kaempferol (K) and quercetin (Q), and two sugar donors, UDP-glucose and UDP-galactose. SlUGT78D-A shows both glucosyltransferase and galactosyltransferase activities at the 3-OH position on kaempferol and quercetin, while SlUGT78D-B exhibits galactosyltransferase activity, but no glucosyltransferase activity. Chromatograms were extracted at a wavelength of 345 nm. **(E)** HPLC chromatograms showing the enzymatic activity of SlUGT79B-B, which produces K-gal-glu (K2) from K-gal using UDP-glucose as sugar donor. SlUGT79B-A does not show this activity. The chromatograms were extracted at a wavelength of 345 nm. **(F)** Working model of transcriptional regulation of UGT enzymes governing distinct flavonol glycoside profiles in pollen and other organs. In most organs except pollen, kaempferol and quercetin are glucosylated by SlUGT78D-A, leading to the formation of flavonol 3-*O*-glucosides (F-glu). Subsequent glycosylation by SlUGT79B-A results in the production of flavonol 3-*O*-rhamnosyl(1→6)glucosides (F-glu-rha; Q4, K4)[24]. In pollen, galactosylation becomes predominant due to the activation of SlUGT78D-B and the repression of SlUGT78D-A. This switch leads to the production of kaempferol 3-*O*-galactoside (K-gal). Further modification by SlUGT79B-B results in kaempferol 3-*O*-glucosyl(1→2)galactoside (K2), which is uniquely abundant in pollen. Abbreviations are K, kaempferol; Q, quercetin; UDP-Glu, UDP-glucose; UDP-Gal, UDP-galactose; glu, glucose; gal, galactose; rha, rhamnose.
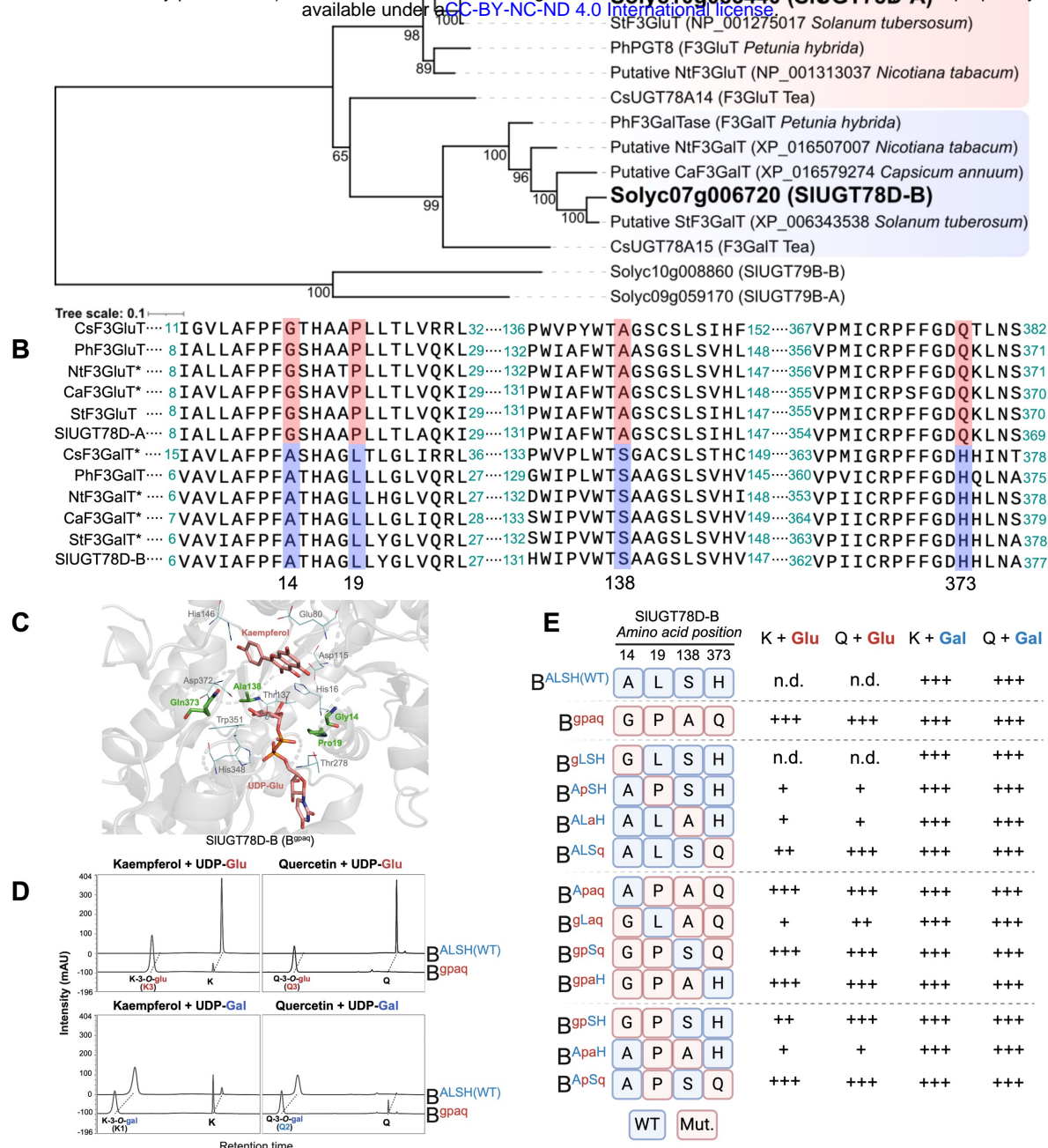
**Fig. 3. Identification of key amino acids that determine the sugar specificity of SlUGT78D-B.**
(A) Phylogenetic analysis with SlUGT78D-A and SlUGT78D-B homologs reveals two distinct clades, the SlUGT78D-A group and the SlUGT78D-B group, highlighted in red and blue, respectively. The tree was constructed using the maximum likelihood method with a bootstrap analysis of 1000 replicates, using the WAG with Freqs. (+F) model. Tomato F3GGT enzymes, SlUGT79B-B and SlUGT79B-A, are used as the outgroup.
(B) Sequence alignment of F3GTs showing four amino acid residues conserved in each group, highlighted in red for the SlUGT78D-A group and blue for the SlUGT78D-B group. The conserved residues are located at positions 14, 19, 138, and 373 of the SlUGT78D-B. (C) A structural model of SlUGT78D-B (B$^{gpaq}$), in which residues 14, 19, 138, and 373 were substituted with those from SlUGT78D-A, was generated with ColabFold[91] and visualized with PyMOL2.5. The substituted amino acids are highlighted in green. The ligand position was determined based on the *Vitis vinifera* GT1 (VvGT1) structure (PDB DOI: https://doi.org/10.2210/pdb2C1Z/pdb). (D) HPLC chromatograms showing the activity of wild-type SlUGT78D-B (B$^{ALSH}$) and the modified SlUGT78D-B (B$^{gpaq}$) having four amino acid substitutions. The wild-type enzyme (B$^{ALSH}$) shows galactosyltransferase activity but lacks glucosyltransferase activity. In contrast, the modified SlUGT78D-B (B$^{gpaq}$) acquires glucosyltransferase activity, producing K-3-*O*-glu and Q-3-*O*-glu. The HPLC chromatograms were extracted at a wavelength of 345 nm. (E) Flavonol 3-*O*-glucosyltransferase and galactosyltransferase activities in various SlUGT78D-B proteins, including wild-type SlUGT78D-B (B$^{ALSH}$) and modified SlUGT78D-B variants with amino acid substitutions at positions 14, 19, 138, or 373 replacing the original residues with those corresponding to SlUGT78D-A. The relative abundance of product peak area in HPLC analysis is marked with '+' (more '+' indicates higher activity). "n.d." indicates not detected.
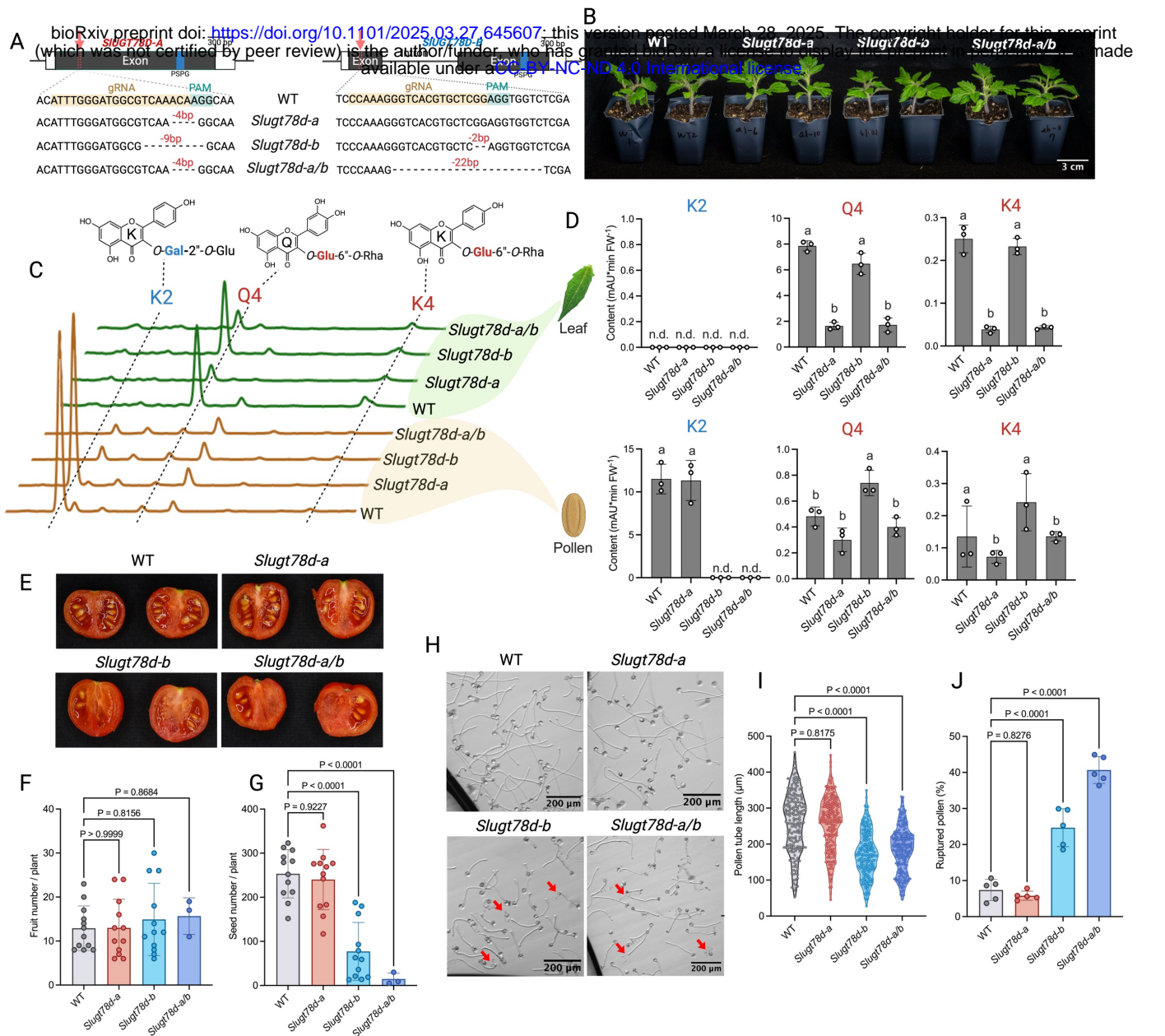
**Fig. 4. Biochemical and developmental characterization of tomato *F3GT* mutants.**

**(A)** Schematic representation of the gene structures of *SlUGT78D-A* and *SlUGT78D-B*. The PSPG motif is marked on gene structures with a blue box. The guide RNA (gRNA) binding sites and the protospacer adjacent motif (PAM) are highlighted in yellow and green, respectively. The resulting deletion mutations in the mutant lines (*Slugt78d-a*, *Slugt78d-b*, and *Slugt78d-a/b*) are indicated. Sequencing chromatograms are shown in Supplementary Figure S7. **(B)** A representative photo of 3-week-old wild type (WT), *Slugt78d-a*, *Slugt78d-b*, and *Slugt78d-a/b*. Scale bar = 3 cm. **(C)** Representative HPLC chromatograms of methanolic extracts from leaves (green traces) of 4-week-old wild type (WT), *Slugt78d-a*, *Slugt78d-b*, and *Slugt78d-a/b* mutants and their pollen grains (brown traces). The retention times for kaempferol 3-O-glucosyl(1→2)galactoside (K2), quercetin 3-O-rhamnosyl(1→6)glucoside (Q4), and kaempferol 3-O-rhamnosyl(1→6)glucoside (K4) are indicated on the chromatogram. **(D)** Concentration of K2, Q4 and K4 is shown as peak area per fresh weight (mAU*min FW$^{-1}$). Data represent mean ± SD (n=3). Statistical significance was determined using one-way ANOVA, followed by Tukey's post-hoc test, with different letters indicating significant differences among groups (P-value < 0.05). Each data point is shown as an open circle on the bar graph. n.d. indicates not detected. **(E)** Cross-sectioned fruits of WT, *Slugt78d-a*, *Slugt78d-b*, and *Slugt78d-a/b*. **(F,G)** The number of fruits per plant (f), and the number of seeds per plant (g) are shown. Data represent mean ± SD (n=12 except *Slugt78d-a/b*, where n=3). **(H)** Microscopic images of growing pollen tubes of WT, *Slugt78d-a*, *Slugt78d-b*, and *Slugt78d-a/b*. Red arrows indicate ruptured pollen tubes. Scale bar = 200 μm. **(I)** Pollen tube length in WT and mutants (n = 200). **(J)** The percentage of ruptured pollens in approximately 100 pollen grains. Data represent mean ± SD (n=5) of five replicates with each replicate containing approximately 100 pollen grains. **(F,G,I,J)** Statistical significance was determined using one-way ANOVA, followed by Dunnett's multiple comparisons test, with adjusted P-values marked at the top.
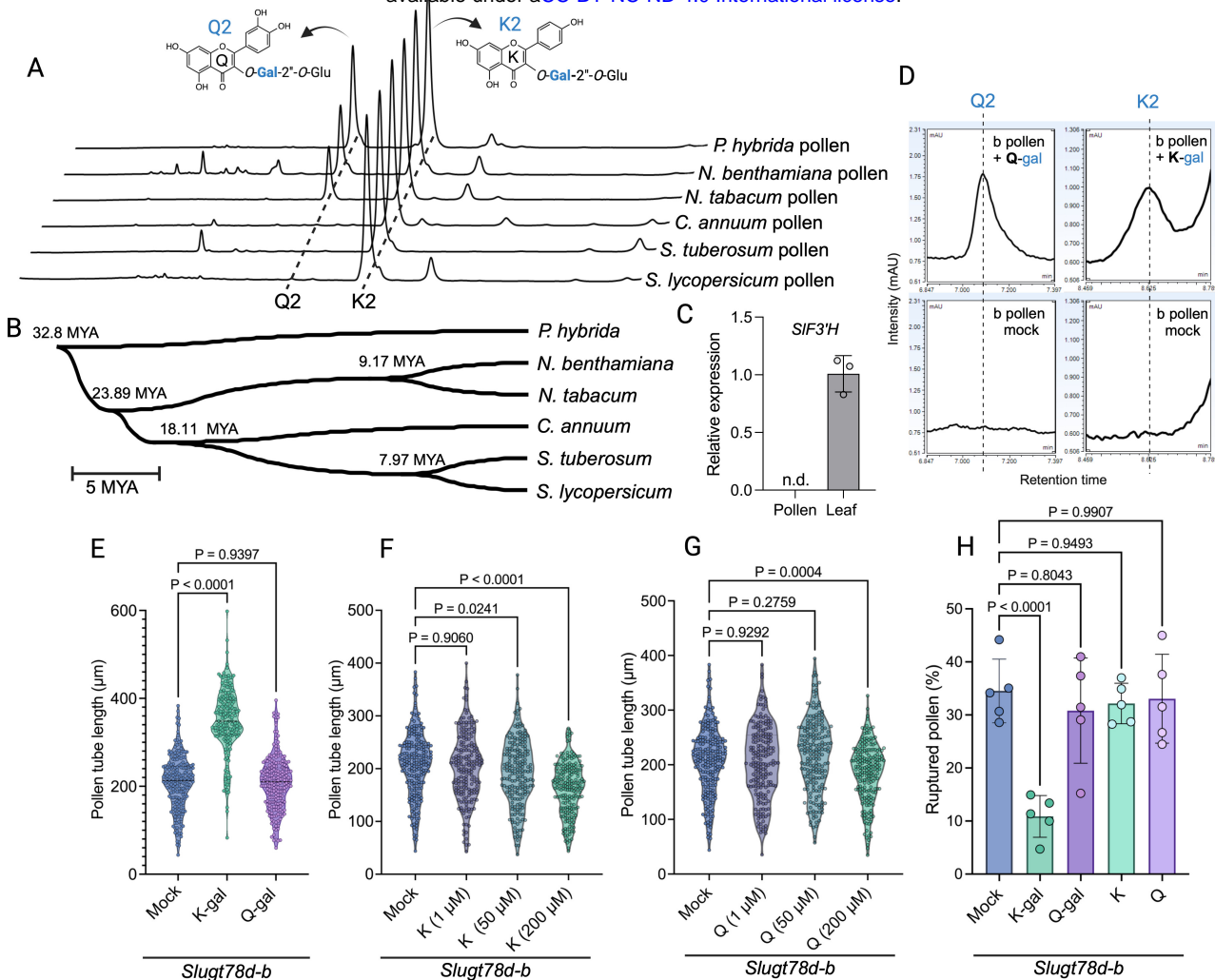
**Fig. 5. Restored pollen tube growth with kaempferol galactosides, but not with aglycones or quercetin galactosides.**
**(A)** Two flavonol galactosides, quercetin 3-*O*-glucosyl(1→2)galactoside (Q2) and kaempferol 3-*O*-glucosyl(1→2)galactoside (K2), predominantly accumulate in pollen of Solanaceae species including *Petunia hybrida* (*P. hybrida*), *Nicotiana benthamiana* (*N. benthamiana*), *Nicotiana tabacum* (*N. tabacum*), *Capsicum annuum* (*C. annuum*), *Solanum tuberosum* (*S. tuberosum*), and *Solanum lycopersicum* (*S. lycopersicum*). K2 was detected in all six species, while Q2 was found only in petunia and the two tobacco species. The HPLC chromatograms were obtained at a wavelength of 345 nm. **(B)** Phylogenetic tree depicting speciation within the Solanaceae family, estimated divergence times (in millions of years ago, MYA) for the Solanaceae species shown in (a). Divergence times are labeled at each node. The phylogenetic tree was retrieved from TimeTree (https://timetree.org). The scale bar represents 5 million years (MYA). **(C)** The relative expression of *SlF3'H* in pollen and leaf, measured by qRT-PCR. Expression levels were normalized to *SlPP2Acs* (*Solyc05g006590*) as an internal control. Data are presented as mean ± SD (n = 3). n.d. indicates that the expression was not detected. **(D)** The production of flavonol diglycosides (K2, Q2) in *Slugt78d-b* pollen when flavonol monoglycosides (K-gal, and Q-gal) were supplied. HPLC chromatograms show the conversion of kaempferol 3-*O*-galactoside (K-gal) to kaempferol 3-*O*-glucosyl(1→2)galactoside (K2) in the right panel, and quercetin 3-*O*-galactoside (Q-gal) to quercetin 3-*O*-glucosyl(1→2)galactoside (Q2) in the left panel. *Slugt78d-b* pollen was treated with 200 μM flavonol monoglycosides in PGM medium for 4 hours, followed by methanolic extraction. Q2 or K2 was not detected in DMSO-treated *Slugt78d-b* pollen (mock). Chromatograms were extracted at a wavelength of 345 nm. **(E)** The pollen tube length (n = 200) of *Slugt78d-b* pollen treated with 200 μM kaempferol 3-*O*-galactoside (K-gal) and quercetin 3-*O*-galactoside (Q-gal) or an equivalent volume of DMSO (mock). **(F, G)** The pollen tube length of *Slugt78d-b* pollen treated with kaempferol (K) and quercetin (Q) aglycones at varying concentrations (1 μM, 50 μM, and 200 μM) (n = 200). **(H)** Bar graph illustrating the percentage of ruptured pollen tubes in *Slugt78d-b* pollen supplemented with 200 μM flavonols or an equivalent amount of DMSO (mock). Each replicate contained approximately 100 pollen grains (n = 5). **(E-H)** Statistical significance was determined using one-way ANOVA followed by Dunnett's multiple comparisons test, with adjusted P-values displayed above the comparisons. Each data point is represented by a circle on the violin or bar graphs.
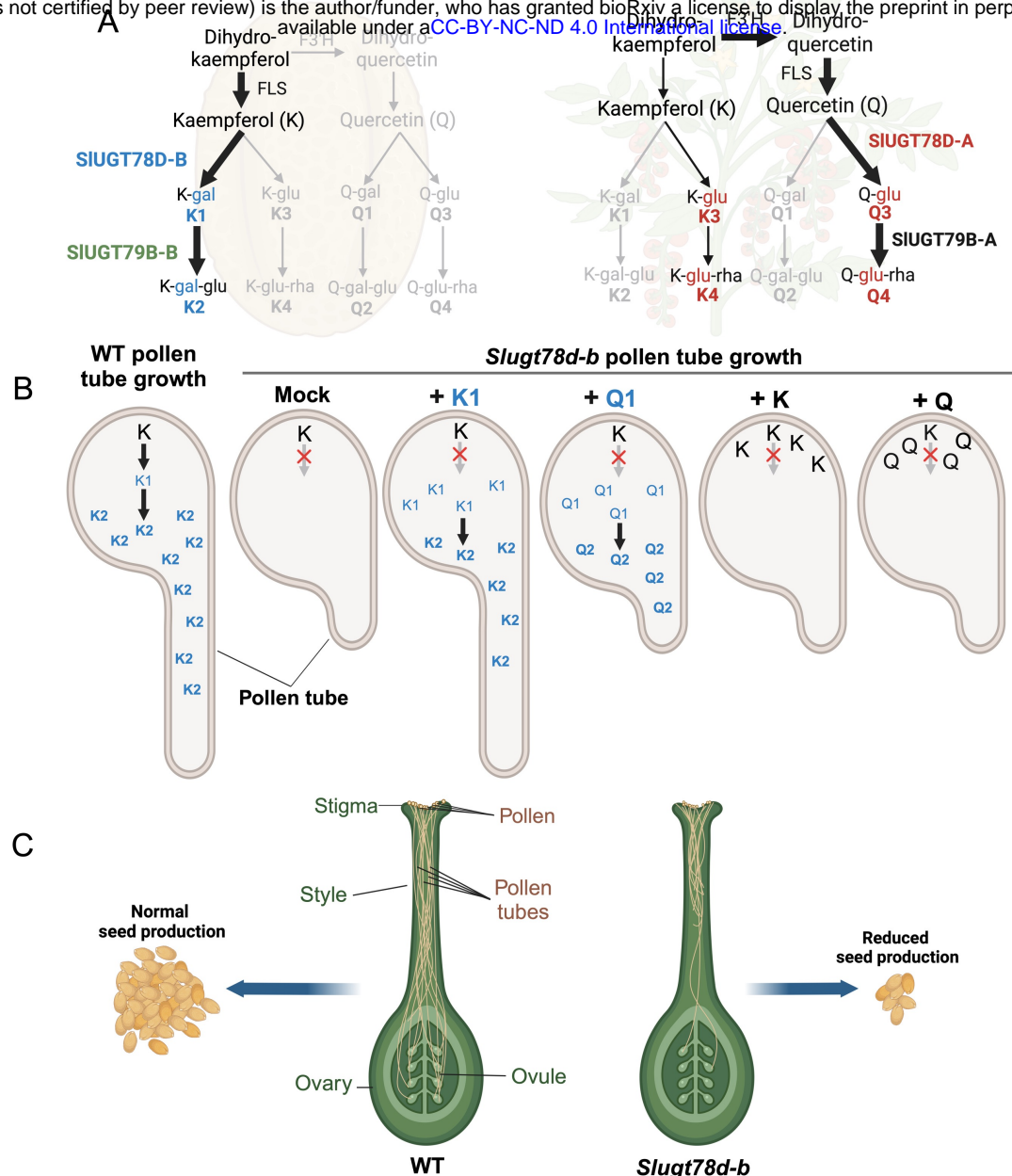
**Fig. 6. A working model illustrates the biosynthesis of flavonol glycosides and their physiological significance in male fertility**

**(A)** Organ-specific flavonol glycoside production in tomato. In pollen, kaempferol (K) is synthesized from dihydrokaempferol via flavonol synthase (FLS), while quercetin production is repressed due to the suppression of *F3'H* expression. The galactosyltransferase SlUGT78D-B catalyzes the formation of kaempferol 3-*O*-galactoside (K-gal, K1), which is further modified by SlUGT79B-B to produce kaempferol 3-*O*-glucosyl(1→2)galactoside (K-gal-glu, K2), a pollen-specific flavonol glycoside. In other organs, both kaempferol (K) and quercetin (Q) are produced via FLS, with F3'H catalyzing the conversion of dihydrokaempferol to dihydroquercetin, a precursor of quercetin. These flavonols are glycosylated by SlUGT78D-A to form kaempferol 3-*O*-glucoside (K-glu, K3) and quercetin 3-*O*-glucoside (Q-glu, Q3). Further modification by SlUGT79B-A produces kaempferol 3-*O*-rhamnosyl(1→6)glucoside (K-glu-rha, K4) and quercetin 3-*O*-rhamnosyl(1→6)glucoside (Q-glu-rha, Q4). Q4 accumulates predominantly in most organs. **(B)** Schematic illustration of defective pollen tube growth in *Slugt78d-b*, which can be chemically complemented with K1 supplementation. In wild-type (WT) pollen, kaempferol (K) undergoes glycosylation to form K1 (kaempferol 3-*O*-galactoside) and K2 (kaempferol 3-*O*-glucosyl(1→2)galactoside. In *Slugt78d-b* mutant pollen, the absence of K1 and K2 results in defective pollen tube growth. Among the tested compounds, only K1 successfully rescued the pollen tube growth. **(C)** In WT plants, pollen tubes grow through the style, delivering male genetic material to the ovules in the ovary, resulting in normal seed production. In contrast, *Slugt78d-b* pollen exhibits defective pollen tube growth, impairing fertilization and significantly reducing seed production. This schematic shows the critical role of specific galactosylated kaempferol in pollen tube development
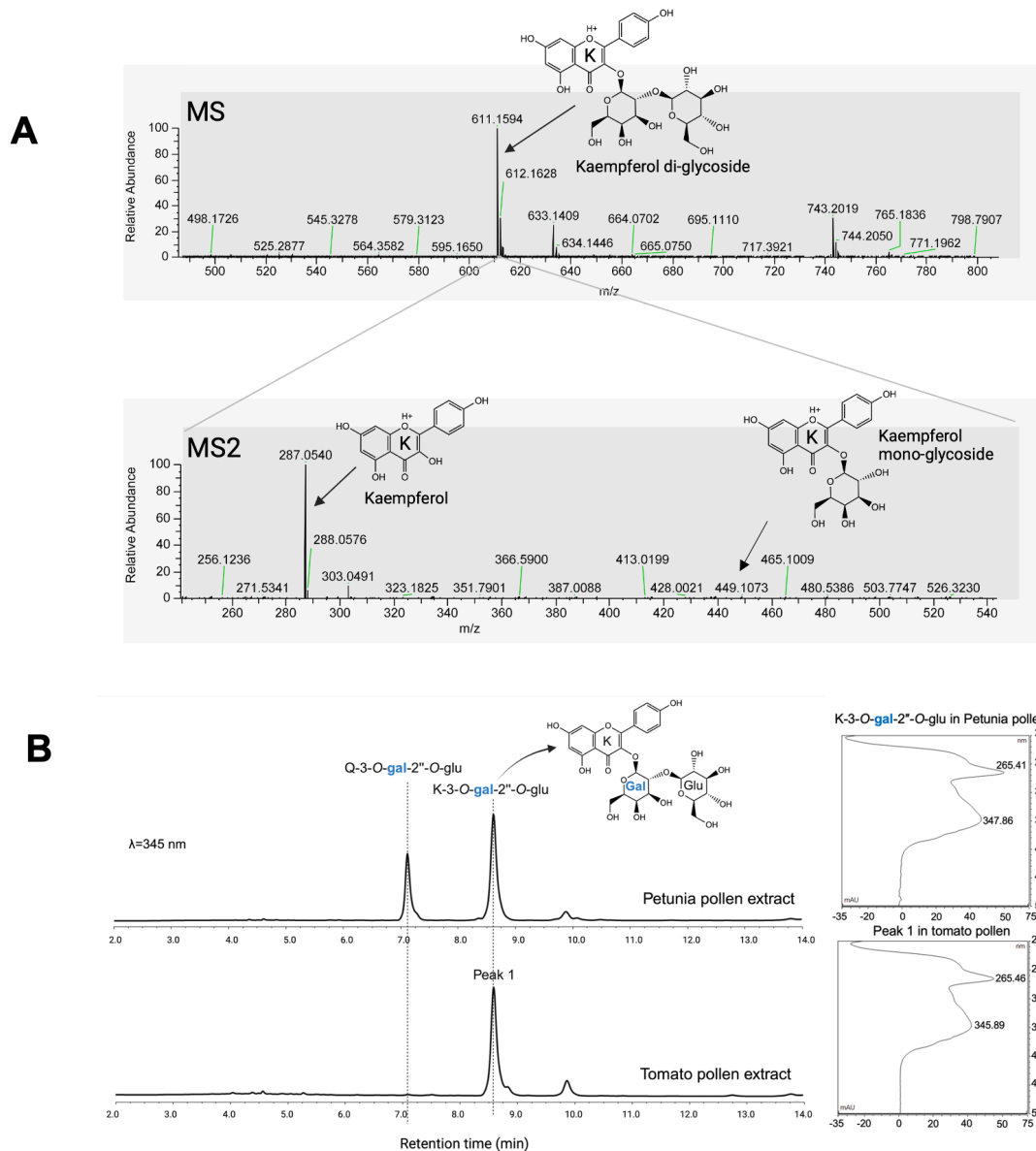
**Figure S1. Identification of a pollen specific kaempferol 3-$O$-glucosyl(1 → 2)galactoside in tomato pollen grains.**

**(A)** LC-MS analysis of the isolated peak from HPLC, which predominantly appears in pollen. MS and MS2 spectra indicate it as a kaempferol di-glycoside containing two hexose units. The MS spectrum displays the precursor ion in positive mode with an m/z of 611.1594, corresponding to kaempferol di-glycoside. The calculated exact mass is 610.1521 Da, determined by subtracting the proton mass (1.0073 Da) from the m/z value. The MS2 spectrum shows the fragmentation pattern, highlighting the major fragment ions, including kaempferol (m/z 287.0540) and kaempferol galactoside or

11  glucoside (m/z 465.1009). **(B)** HPLC chromatograms and UV spectra of pollen extracts

12  from Petunia and tomato. The UV spectra and retention time of the tomato pollen peak

13  (Peak 1) match with the most abundant flavonol of petunia pollen, which was identified

14  as either kaempferol or quercetin 3-*O*-glucosyl(1 → 2)galacoside (K/Q-3-*O*-gal-2"-*O*-

15  glu) in a previous report(*1*). Taken together with mass data and profile comparison with

16  Petunia pollen, we concluded that Peak 1 is kaempferol 3-*O*-glucosyl(1 → 2)

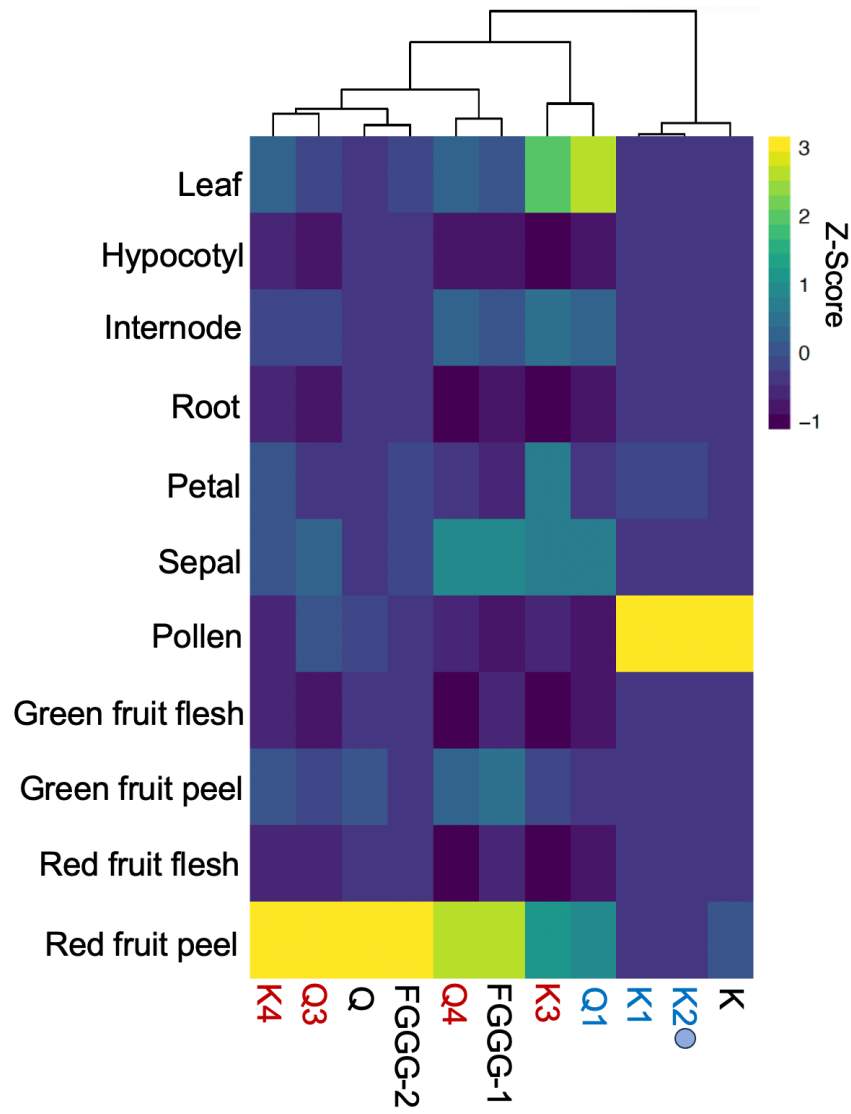17  galactoside (K2; K-3-*O*-gal-2"-*O*-glu).

18

19

**Figure S2. Heatmap of flavonol glycosides across tomato organs detected with LC-MS.** The heatmap displays the relative abundance (Z-score) of various flavonol glycosides and two aglycones, K and Q, across different tomato organs. Each column represents a specific flavonol, and the Z-score indicates its relative abundance across different tomato organs. K, K1, and K2 are almost exclusively detected in pollen grains. K2 is the compound with a calculated exact mass of 610.1534, corresponding to the Peak 1, identified in Supplementary Figure S1. The raw data for this LC-MS analysis is available in Supplementary Table S1.

*SlF3'H* (*Solyc03g115220*) expression profile

28

**Figure S3. Gene expression profile of *SlF3'H* (*Solyc03g115220*).**

The raw transcript per million (TPM) data were obtained from the public transcriptome database CoNekT (https://conekt.sbs.ntu.edu.sg). The graph shows the minimal expression of SlF3'H in pollen grains and at different stages of pollen tube development.

| | 1. | 2. | 3. | 4. | 5. | 6. | 7. | 8. | 9. | 10. | 11. | 12. |
|---|---|---|---|---|---|---|---|---|---|---|---|---|
| 1. CsF3GluT (CsUGT78A14 *Camellia sinensis*) | 100 | | | | | | | | | | | |
| 2. Putative CaF3GluT (KAF3646237 *Capsicum annuum*) | 55.6 | 100 | | | | | | | | | | |
| 3. StF3GluT (NP_001275017 *Solanum tuberosum*) | 55.3 | 84.8 | 100 | | | | | | | | | |
| 4. SlUGT78D-A (Solyc10g083440) | 55.1 | 82.7 | 93.5 | 100 | | | | | | | | |
| 5. PhF3GluT (PGT8 *Petunia hybrida*) | 55.2 | 77.9 | 79.4 | 78 | 100 | | | | | | | |
| 6. Putative NtF3GluT (NP_001313037 *Nicotiana tabacum*) | 56.3 | 83.5 | 82.1 | 79.4 | 83.5 | 100 | | | | | | |
| 7. CsF3GalT (UGT78A15 *Camellia sinensis*) | 53.8 | 48.7 | 47.8 | 47.2 | 48.4 | 49.3 | 100 | | | | | |
| 8. PhF3GalT (F3GalTase *Petunia hybrida*) | 52.6 | 52.3 | 50.9 | 51 | 51 | 52.1 | 64.7 | 100 | | | | |
| 9. Putative NtF3GalT (XP_016507007 *Nicotiana tabacum*) | 51.9 | 50.5 | 50 | 50.6 | 50.1 | 49.8 | 62.8 | 82.9 | 100 | | | |
| 10. Putative CaF3GalT (XP_016579274 *Capsicum annuum*) | 49.3 | 49.1 | 48.6 | 49.4 | 49 | 49.7 | 58.6 | 76.2 | 77.7 | 100 | | |
| 11. Putative StF3GalT (XP_006343538 *Solanum tuberosum*) | 48.6 | 47.5 | 46.3 | 47.1 | 47.6 | 47.6 | 58.4 | 75.6 | 78.7 | 81 | 100 | |
| 12. SlUGT78D-B (Solyc07g006720) | 49.1 | 49.2 | 47.8 | 48.9 | 47.7 | 48.6 | 58.1 | 74.9 | 76.8 | 79.4 | 92 | 100 |

**Figure S4. Homologs of flavonol 3-*O*-glycosyltransferase enzymes (SlUGT78D-A and SlUGT78D-B) in other Solanaceae species.**

A heatmap displaying the percentage identity of protein sequences among SlUGT78D-A, SlUGT78D-B, their homologs in four Solanaceae species, *Nicotiana tabacum*, *Capsicum annuum*, *Solanum tuberosum*, *Petunia x hybrida,* and CsUGT78A14 and CsUGT78A15 from *Camellia sinensis*. Flavonol 3-*O*-glucosyltransferase (CsUGT78A14) and flavonol 3-*O*-galactosyltransferase (CsUGT78A15) from *Camellia sinensis* (tea) are also included in this comparison. High identity percentages suggest functional conservation.
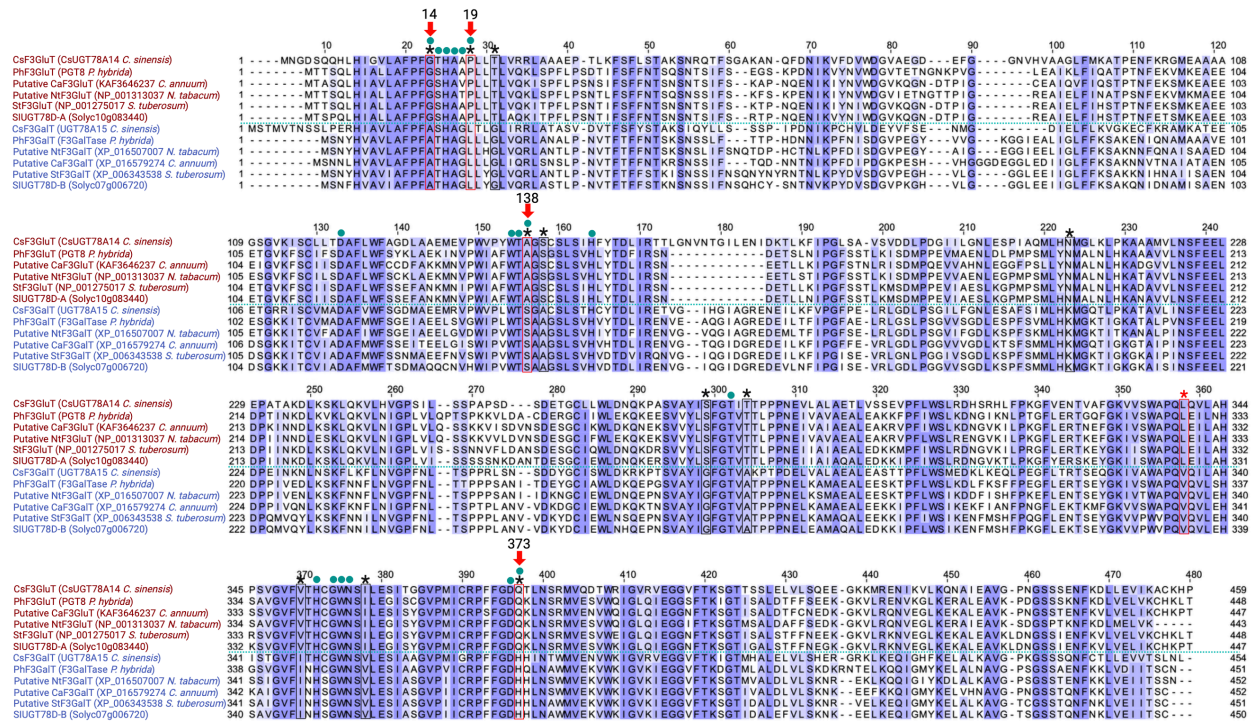
49

**Figure S5. Protein sequence alignment of F3GTs.**

Sequence alignment of F3GT enzymes from various species, including *Petunia x hybrida, Nicotiana tabacum, Capsicum annuum, Solanum lycopersicum, Solanum tuberosum,* and *Camellia sinensis*. Amino acids highlighted in blue represent conserved residues, based on the BLOSUM62 score. Among these conserved amino acids, 11 amino acids are uniquely conserved in the SlUGT78D-A group and the SlUGT78D-B group, marked with asterisks. Green circles indicate amino acid positions predicted to protrude into ligand binding sites, as inferred from the GT1 structure (*Vitis vinifera*)(*2, 3*). Red arrows mark the four amino acids identified in this study as essential for sugar specificity.
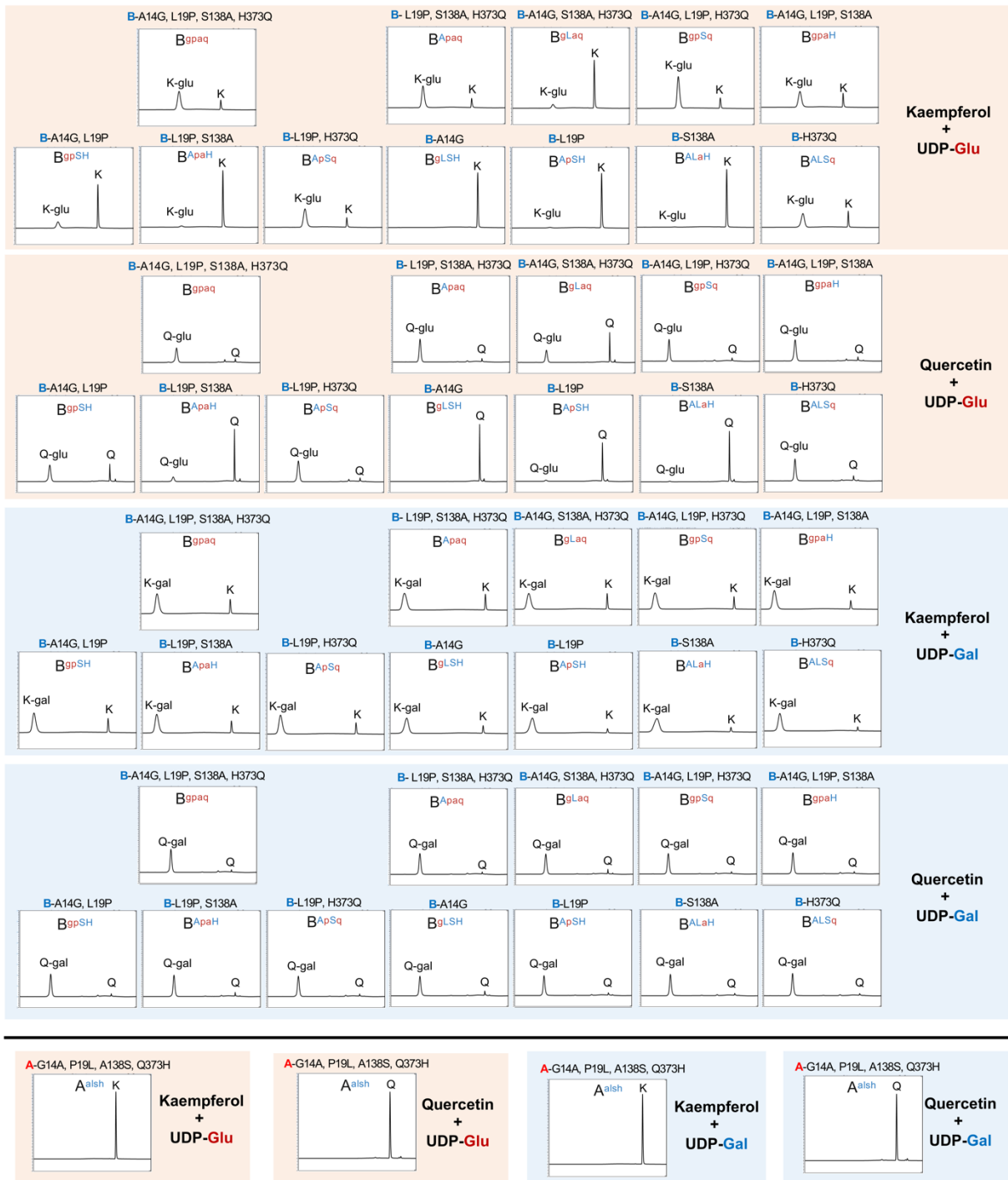
**Figure S6. Enzyme activities of modified F3GT enzymes.**

HPLC chromatograms representing the enzymatic activity of modified F3GT enzymes. The upper panels depict activities of SlUGT78D-B mutant variants, while the lower panels show flavonol 3-*O*-glucosyltransferase or 3-*O*-galactosyltransferase activities of the SlUGT78D-A$^{alsh}$ mutant. The activity was tested using two substrates, kaempferol

67  (K) or quercetin (Q), in the presence of UDP-glucose (UDP-Glu) or UDP-galactose

68  (UDP-Gal) as sugar donors. Each chromatogram represents a different combination of

69  enzymes, aglycones (K or Q), and sugar donors (Glu or Gal). The chromatograms were

70  obtained at a wavelength of 345 nm, showing the resulting flavonol glycosides produced

71  under each condition. K-glu: Kaempferol 3-*O*-glucoside, K-gal: Kaempferol 3-*O*-

72  galactoside, Q-glu: Quercetin 3-*O*-glucoside, Q-gal: Quercetin 3-*O*-galactoside.
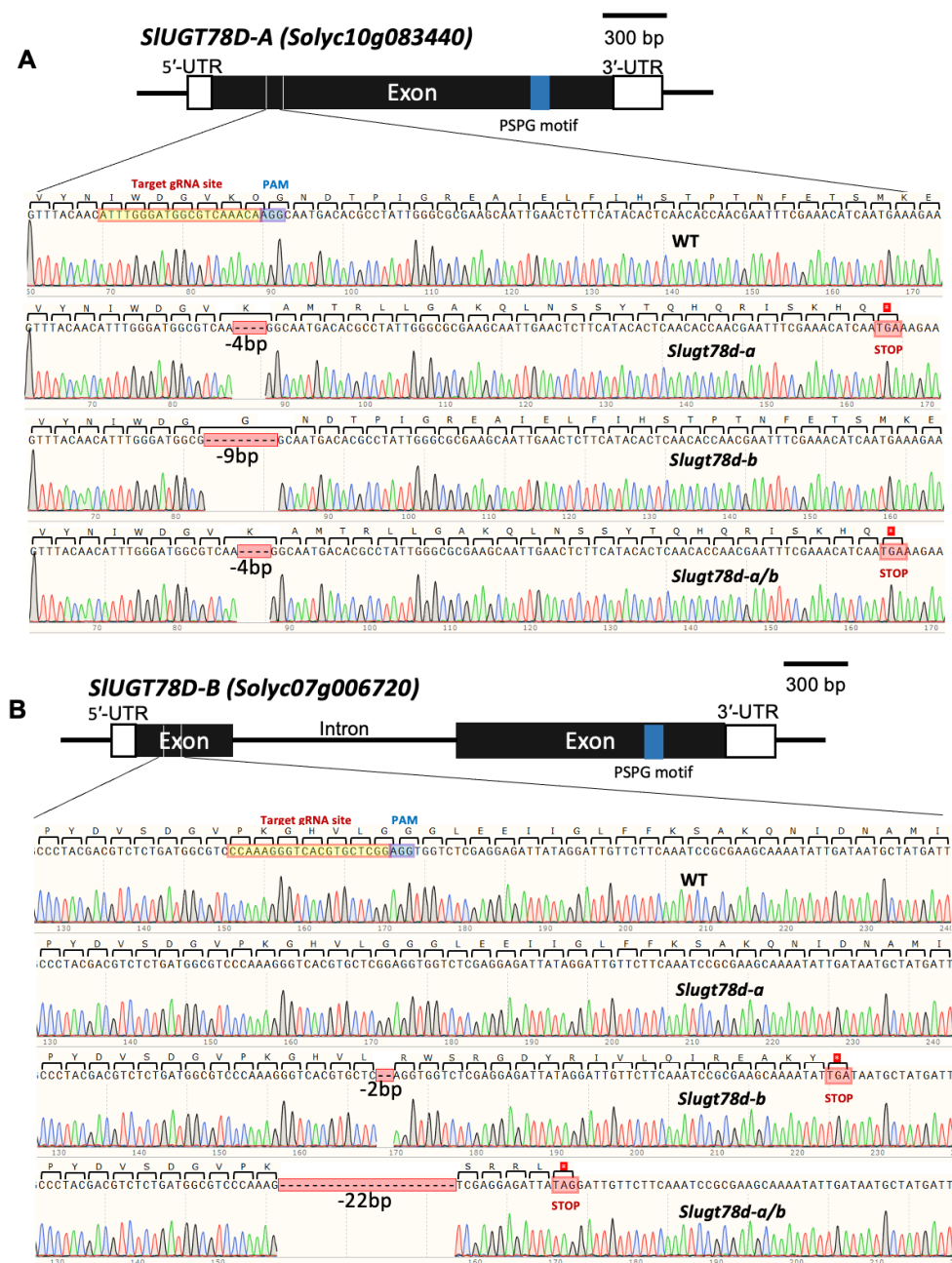
73

74

**Figure S7. Generation of *Slugt78d-a*, *Slugt78d-b*, and *Slugt78d-a/b* mutants using the CRISPR-Cas9 system.**

Schematic gene structures of *SlUGT78D-A* (**a**) and *SlUGT78D-B* (**b**) are shown, along with sequencing chromatograms displaying the regions where gene editing occurred. **(A)** *Slugt78d-a* and *Slugt78d-a/b* mutants have a 4 bp deletion in *SlUGT78D-A*, resulting in an early stop codon. *Slugt78d-b* has a 9 bp deletion in *SlUGT78D-A*, but this

81    mutation does not cause a frameshift. **(B)** For *SlUGT78D-B*, the *Slugt78d-b* mutant has

82    a 4 bp deletion, and the *Slugt78d-a/b* mutant has a 22 bp deletion, both of which result

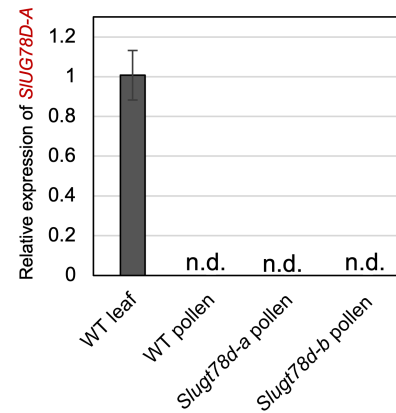83    in early stop codons, disrupting the gene function.

84

**Figure S8. *SlUGT78D-A* is not transcriptionally induced in *Slugt78d-b* pollen.**

Relative expression of *SlUGT78D-A* in wild-type leaf and pollen grains of WT, *Slugt78d-a,* and *Slugt78d-b*, measured using qRT-PCR. Expression levels were normalized using *SlACTIN2* (*Solyc11g005330*) as an internal control. Data represent mean ± SD (n=4). n.d. indicates not detected.
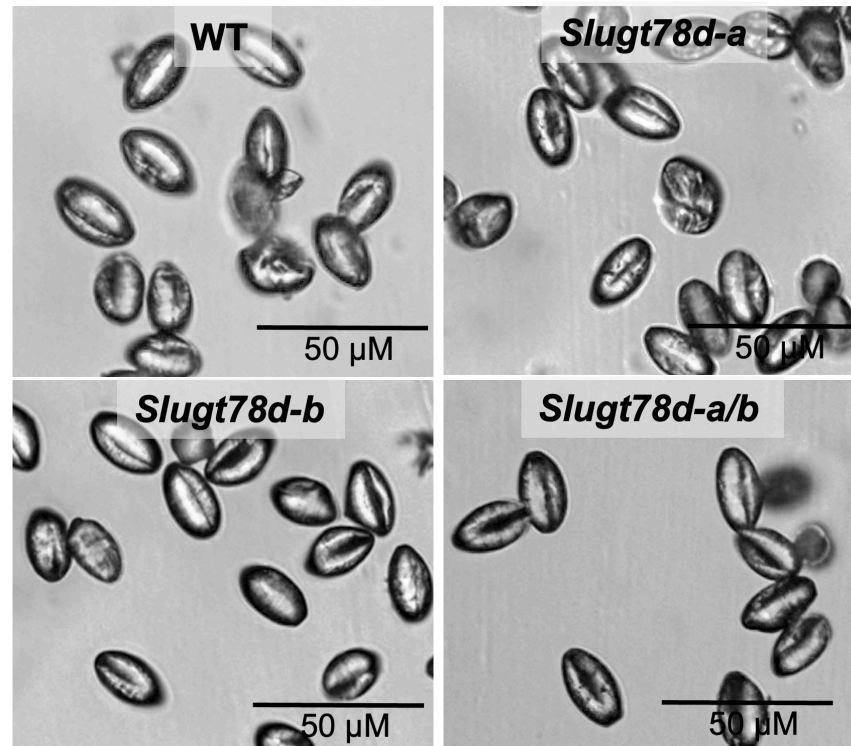
92

**Figure S9. Pollen grain morphology in wild type and three *Slugt78d* mutants.**

Microscopic images of pollen grains from wild type (WT), *Slugt78d-a*, *Slugt78d-b*, and *Slugt78d-a/b*. The images do not show any obvious morphological alterations in the pollen grains of mutants compared to wild type.
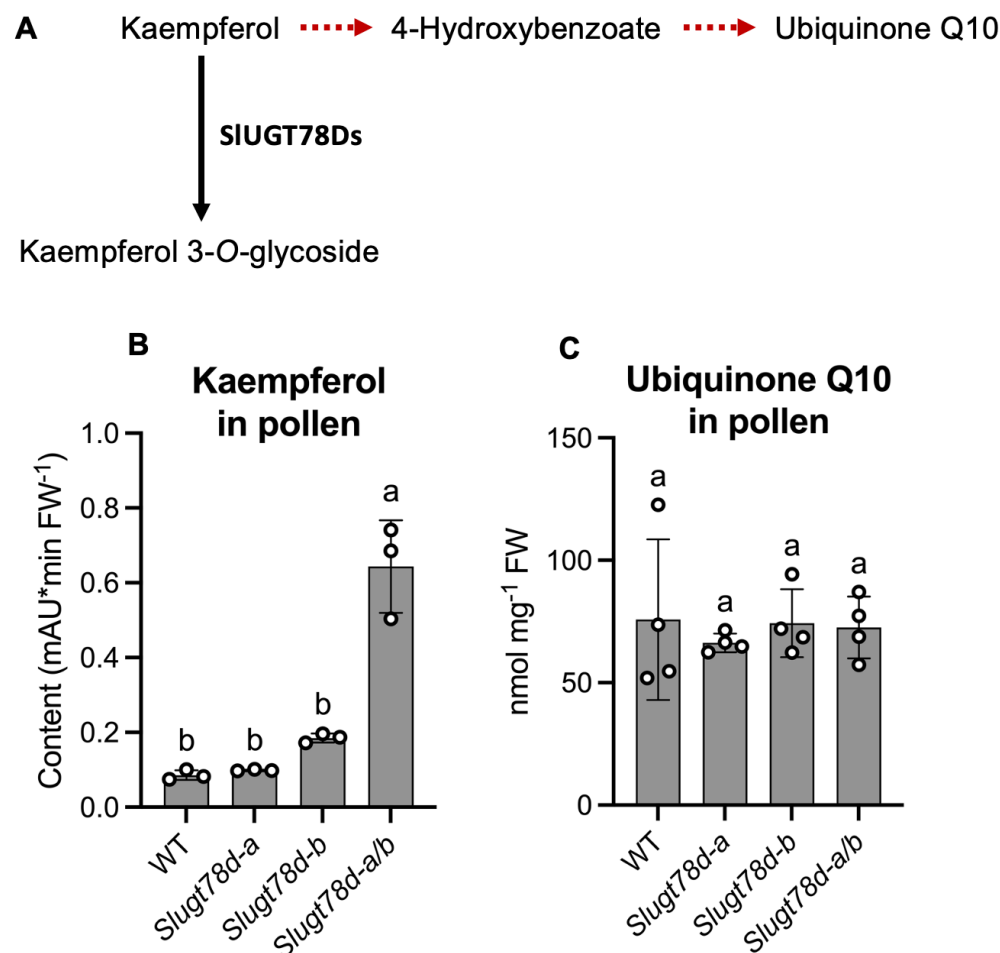
97

**A** Kaempferol ┈▶ 4-Hydroxybenzoate ┈▶ Ubiquinone Q10

SlUGT78Ds

Kaempferol 3-*O*-glycoside

**98**

**99** **Figure S10. Ubiquinone Q10 content in pollen grains.**

**100** **(A)** Schematic diagram shows the biosynthetic pathway of ubiquinone Q10 from

**101** kaempferol as a precursor. **(B)** The levels of free kaempferol in the pollen grains of WT

**102** and three *Slugt78d* mutants. **(C)** The levels of ubiquinone Q10 in the pollen grains of

**103** WT and three *Slugt78d* mutants. **(B, C)** Data represent mean ± SD (n=3). Statistical

**104** significance was determined using one-way ANOVA, followed by Tukey's post-hoc test,

**105** with different letters indicating significant differences among groups (P-value < 0.05).

**106** The metabolite levels were normalized to fresh weight (FW). Each data point is shown

**107** as an open circle on the bar graph.

**108**

| | 1. | 2. | 3. | 4. | 5. | 6. | 7. | 8. | 9. | 10. |
|---|---|---|---|---|---|---|---|---|---|---|
| 1. SlUGT79B-A (Solyc09g059170) | 100 | | | | | | | | | |
| 2. Putative StF3G6"RT (XP_006367560.1 *Solanum tuberosum*) | 95.5 | 100 | | | | | | | | |
| 3. PhF3G6"RT (UGT72 *Petunia hybrida*) | 82.9 | 83.9 | 100 | | | | | | | |
| 4. Putative CaF3G6"RT (XP_016562500.1 *Capsicum annuum*) | 86.1 | 87.9 | 84.9 | 100 | | | | | | |
| 5. Putative NtF3G6"RT (XP_016514239.1 *Nicotiana tabacum*) | 87.6 | 88.6 | 87.9 | 89.2 | 100 | | | | | |
| 6. Putative_CaF3G2"GT (KAF3678162.1 *Capsicum annuum*) | 40.3 | 41.2 | 41.4 | 40.4 | 41.2 | 100 | | | | |
| 7. SlUGT79B-B (Solyc10g008860) | 41.3 | 42.2 | 42 | 41.7 | 42 | 87.4 | 100 | | | |
| 8. Putative StF3G2"GT (XP_006361070.1 *Solanum tuberosum*) | 38.8 | 39.8 | 39.6 | 39.7 | 39.8 | 86.6 | 93.6 | 100 | | |
| 9. PhF3G2"GT (UGT79B31 *Petunia hybrida*) | 40.3 | 41 | 41 | 40.7 | 41.2 | 81.3 | 82.8 | 81.1 | 100 | |
| 10. Putative NtF3G2"GT (XP_016443026.1 *Nicotiana tabacum*) | 38.6 | 39.8 | 40.2 | 39.5 | 40.7 | 84.2 | 84.4 | 83.2 | 86.4 | 100 |

**Figure S11. Homologs of flavonol 3-*O*-glycoside: glycosyltransferase (F3GGT) enzymes (SlUGT79B-A and SlUGT79B-B) in other Solanaceae species.**

A heatmap displaying the percentage identity of protein sequences among SlUGT79B-A, SlUGT79B-B, their homologs in four Solanaceae species, *Nicotiana tabacum*, *Capsicum annuum*, *Solanum tuberosum*, *Petunia x hybrida*. High identity percentages suggest functional conservation.
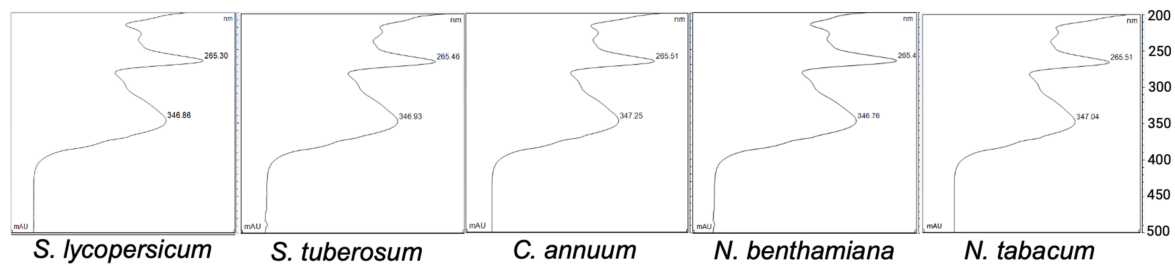
**Figure S12. Conservation of pollen-specific kaempferol 3-*O*-glucosyl(1 → 2)galactoside (K2).**

UV absorbance spectra corresponding to the K2 peaks in pollen extracts from five Solanaceae plants.

124

125



126

**Figure S13. Gene expression profile of *SlFST1* (*Solyc03g113440*), a homolog of Arabidopsis *FST1.***

The raw transcript per million (TPM) data were obtained from the public transcriptome database CoNekT (https://conekt.sbs.ntu.edu.sg). The graph shows the specific high expression of *SlFST1* in pollen grains and at different stages of pollen tube development.

133

134

135

136

137

138

139

140

141

142

143

144 **Table S3. Primer list used in this study.**

| No. | Primer list | Sequence (5' -> 3') | Purpose |
|---|---|---|---|
| 1 | Geno-78DA-F | AGACCTCAAATCAAAGCTCCA | Genotyping |
| 2 | Geno-78DA-R | AGTCTTGACTCCGTTGTCTCT | Genotyping |
| 3 | Geno-78DB-F | AGCATTTCCTTTTGCAACACA | Genotyping |
| 4 | Geno-78DB-R | AGTGATCCAGCTGCAGAAGT | Genotyping |
| 5 | qRT-78DA-F | AAACAAGGCAATGACACGCC | qRT-PCR |
| 6 | qRT-78DA-R | CCCTGTTTCCTCCTCTGCTT | qRT-PCR |
| 7 | qRT-78DB-F | GACTTCTGCAGCTGGATCAC | qRT-PCR |
| 8 | qRT-78DB-R | AACTCCACCAGGCAAATCAC | qRT-PCR |
| 9 | qRT-SlF3'H-F | TTTTCGCACCTTACGGACCA | qRT-PCR |
| 10 | qRT- SlF3'H-R | GCGCGTGTAAGTGTTCTGAC | qRT-PCR |
| 11 | qRT-SlACTIN2-F | TTGCTGACCGTATGAGCAAG | qRT-PCR |
| 12 | qRT-SlACTIN2-R | GGACAATGGATGGACCAGAC | qRT-PCR |
| 13 | qRT-SlPP2Acs-F | CGATGTGTGATCTCCTATGGTC | qRT-PCR |
| 14 | qRT-SlPP2Acs-R | AAGCTGATGGGCTCTAGAAATC | qRT-PCR |

145

146 **Table S4. Protein accession number for phylogenetic tree.**

| Name | Activity | Organism | Accession number |
|---|---|---|---|
| AtUGT78D1 | F3RhaT | *Arabidopsis thaliana* | AT1G30530.1 (TAIR) |
| AtUGT78D2 | F3GluT | *Arabidopsis thaliana* | AT5G17050.1 (TAIR) |
| AtUGT78D3 | F3AraT | *Arabidopsis thaliana* | AT5G17030.1 (TAIR) |
| VvGT1 | F3GluT | *Vitis vinifera* (Grape) | P51094 (UniProt) |
| VvGT5 | F3GAT | *Vitis vinifera* (Grape) | C7G3B5 (UniProt) |
| VvGT6 | F3Glu/GalT | *Vitis vinifera* (Grape) | C7G3B6 (UniProt) |
| PhF3GalTase | F3GalT | *Petunia x hybrida* | Q9SBQ8 (UniProt) |
| PhPGT8 | F3GluT | *Petunia x hybrida* | Q9SBQ3 (UniProt) |
| Sm3GT | F3GluT | *Solanum melongena* (Eggplant) | Q43641 (UniProt) |
| CsUGT78A14 | F3GluT | *Camellia sinensis* (Tea) | A0A109P632 (UniProt) |
| CsUGT78A15 | F3GalT | *Camellia sinensis* (Tea) | A0A0X9I0C6 (UniProt) |
| ZmBZ1 | F3GluT | *Zea mays* (Corn) | P16165 (UniProt) |
| HvBZ1 | F3GluT | *Hordeum vulgare* (Barley) | P14726 (UniProt) |
| AtUGT79B1 | F3G2″XylT | *Arabidopsis thaliana* | AT5G54060.1 (TAIR) |
| AtUGT79B6 | F3G2″GluT | *Arabidopsis thaliana* | AT5G54010.1 (TAIR) |
| PhUGT79B31 | F3G2″GluT | *Petunia x hybrida* | A0A2Z6FLE1 (UniProt) |
| PhUGT72 | F3G6″RhaT | *Petunia x hybrida* | Q43716 (UniProt) |

147

148

**Supplemental References**

1. E. Knoch, S. Sugawara, T. Mori, R. Nakabayashi, K. Saito, K. Yonekura-Sakakibara, UGT79B31 is responsible for the final modification step of pollen-specific flavonoid biosynthesis in Petunia hybrida. *Planta* **247**, 779–790 (2018).

2. W. Offen, C. Martinez-Fleites, M. Yang, E. Kiat-Lim, B. G. Davis, C. A. Tarling, C. M. Ford, D. J. Bowles, G. J. Davies, Structure of a flavonoid glucosyltransferase reveals the basis for plant natural product modification. *EMBO J.* **25**, 1396–1405 (2006).

3. E. Ono, Y. Homma, M. Horikawa, S. Kunikane-Doi, H. Imai, S. Takahashi, Y. Kawai, M. Ishiguro, Y. Fukui, T. Nakayama, Functional differentiation of the glycosyltransferases that contribute to the chemical diversity of bioactive flavonol glycosides in grapevines (Vitis vinifera). *Plant Cell* **22**, 2856–2871 (2010).